(2)

PL-TR-92-2109

QUANTIFICATION OF m_{Lg} FOR SMALL EXPLOSIONS

R. B. Herrmann
G. Al-Eqabi
K. Hutchensen

St. Louis University
Department of Earth & Atmospheric Sciences
3507 Laclede Avenue
St. Louis, MO 63103

23 April 1992

Scientific Report No. 1

PHILLIPS LABORATORY
AIR FORCE SYSTEMS COMMAND
HANSCOM AIR FORCE BASE, MASSACHUSETTS 01731-5000

The views and conclusions contained in this document are those of the authors and should not be interpreted as representing the official policies, either expressed or implied, of the Air Force or the U.S. Government.

This technical report has been reviewed and is approved for publication.

JAMES F. LEWKOWICZ
Contract Manager
Solid Earth Geophysics Branch
Earth Sciences Division

JAMES F. LEWKOWICZ
Branch Chief
Solid Earth Geophysics Branch
Earth Sciencs Division

DONALD H. ECKHARDT, Director
Earth Sciences Division

This document has been reviewed by the ESD Public Affairs Office (PA) and is releasable to the National Technical Information Service (NTIS).

Qualified requestors may obtain additional copies from the Defense Technical Information Center. All others should apply to the National Technical Information Service.

If your address has changed, or if you wish to be removed from the mailing list, or if the addressee is no longer employed by your organization, please notify PL/IMA, Hanscom AFB MA 01731-5000. This will assist us in maintaining a current mailing list.

Do not return copies of this report unless contractual obligations or notices on a specific document requires that it be returned.

REPORT DOCUMENTATION PAGE

Form Approved
OMB No. 0704-0188

1. AGENCY USE ONLY *(Leave blank)*	2. REPORT DATE	3. REPORT TYPE AND DATES COVERED
	23 April 1992	Scientific Report No. 1

4. TITLE AND SUBTITLE

Quantification of m_{Lg} for Small Explosions

5. FUNDING NUMBERS

PE 62101F
PR 7600 TA 09 WU BC

Contract F19628-90-K-0040

6. AUTHOR(S)

R. B. Herrmann
G. Al-Eqabi
K. Hutchensen

7. PERFORMING ORGANIZATION NAME(S) AND ADDRESS(ES)

St Louis University
Department of Earth & Atmospheric Sciences
3507 Laclede Avenue
St Louis, MO 63103

8. PERFORMING ORGANIZATION REPORT NUMBER

9. SPONSORING/MONITORING AGENCY NAME(S) AND ADDRESS(ES)

Phillips Laboratory
Hanscom AFB, MA 01731-5000

Contract Manager: James Lewkowicz/GPEH

10. SPONSORING/MONITORING AGENCY REPORT NUMBER

PL-TR-92-2109

11. SUPPLEMENTARY NOTES

12a. DISTRIBUTION/AVAILABILITY STATEMENT

Approved for public release;
Distribution unlimited

12b. DISTRIBUTION CODE

13. ABSTRACT *(Maximum 200 words)*

This report focuses on a USGS data set from refraction surveys within the State of Maine. These data contain excellent recordings of short period Rayleigh waves (Rg) generated by the explosions. The initial intent was to use these data to characterize shear wave velocity and Q in the upper 1-2 km in this environment of folded paleozoic sediments. However the data set permitted other interesting studies.

First, significant lateral changes in the moveout of the Rg, S and P wave were observed. Analysis techniques were developed to successfully invert for a laterally varying earth structure and to model the Rg waveforms, both in terms of absolute amplitude and phase.

Second, the shear wave velocity model derived from the surface waves, was used in a blind test to predict the S-wave arrival times for two profiles having significant S waves. An excellent fit was obtained without having used the S-wave data in the inversion for the earth model, indicating the ability of the 1-4 Hz surface wave data to resolve shear wave velocity structure to depths of 2 km in this environment.

Finally, since absolute instrument gains were known, forward modeling was used to compare the observed and estimated amplitude decay in different frequency bands. This permitted an estimation of the isotropic moment for these one ton explosions. By comparing estimates made in different portions of the 1-5 Hz frequency band, we conclude that a step source time function in moment is adequate to model the surface wave observations for these one ton shots. The estimated isotropic moments are similar to other chemical yield-moment observations. However, larger industrial chemical blasts, e.g., 100 ton or greater, would be expected to show a frequency dependence in the isotropic moment estimate because of the distributed source dimensions.

14. SUBJECT TERMS

Explosions
Seismic Waves
Moment

15. NUMBER OF PAGES

58

16. PRICE CODE

17. SECURITY CLASSIFICATION OF REPORT	18. SECURITY CLASSIFICATION OF THIS PAGE	19. SECURITY CLASSIFICATION OF ABSTRACT	20. LIMITATION OF ABSTRACT
Unclassified	Unclassified	Unclassified	SAR

CONTENTS

Preface iv

Surface Wave Inversion for Shear Wave Velocity..... 1

Ground Roll: A Potential Tool for Constraining Shear Wave Statics 13

Geophysical Techniques for Characterizing Shallow Velocity Attenuation Models 26

Isotropic Moment - Yield Relations for Small Chemical Explosions 39

Preface

This report focuses on a USGS provided data set from refraction surveys within the State of Maine. These data contain excellent recordings of short period Rayleigh waves (Rg) generated by the explosions. The initial intent was to use these data to characterize shear wave velocity and Q in the upper 1-2 km in this environment of folded paleozoic sediments. However the data set exhibited interesting wave propagation characteristics. The principle results of the study are as follow:

First, significant lateral changes in the moveout of the Rg, S and P wave were observed. Analysis techniques were developed to successfully invert for a laterally varying earth structure and to model the Rg waveforms, both in terms of absolute amplitude and phase.

Second, the shear wave velocity model derived from the surface waves, was used in a blind test to predict the S-wave arrival times for two profiles having significant S waves. An excellent fit was obtained without having used the S-wave data in the inversion for the earth model. This indicated the ability of the 1-4 Hz surface wave data to resolve shear wave velocity structure to depths of 2 km in this environment.

Finally, since absolute instrument gains were known, forward modeling was used to test the laterally varying velocity and Q model, in order to compare the observed and estimated amplitude decay in different frequency bands. This permitted an estimation of the isotropic moment for these one ton explosions. By comparing estimates made in different portions of the 1-5 Hz frequency band, we conclude that a step source time function in moment is adequate to model the surface wave observations for these one ton shots. The estimated isotropic moments are similar to other chemical yield-moment observations. However, larger industrial chemical blasts, e.g., 100 ton or greater, would be expected to show a frequency dependence in the isotropic moment estimate because of the distributed source dimensions.

These report presents the data sets and conclusions in four sections.

SURFACE WAVE INVERSION FOR SHEAR WAVE VELOCITY

R. B. HERRMANN and G. I. AL-EQABI

Department of Earth and Atmospheric Sciences
Saint Louis University
3507 Laclede Avenue
St. Louis, Missouri 63103

ABSTRACT

Land based seismic exploration has typically viewed the surface wave or ground roll as undesirable noise while earthquake seismology has been able to use the surface wave to invert for lateral variations in crust-upper mantle shear-wave velocity. Although surface-wave inversion techniques for shear-wave velocity and shear-wave Q are easy to apply once the phase velocity, group velocity and anelastic attenuation dispersion are known, the manner in which these parameters are obtained efficiently from large exploration data sets has not been fully explored. This paper will address the processing steps required and apply them to surface-waves recorded in a refraction experiment in the State of Maine in the U. S.

INTRODUCTION

In earthquake seismology, surface waves have long been used to infer shear wave velocity models of the crust and upper mantle of the earth (Ewing *et al.*, 1957). Analysis techniques have been developed to invert for shear velocity as a function of depth, and recently progress has been made in using these data to invert for lateral variations in earth structure (Nolet, 1987; Nolet, 1990). On the other hand, less attention has been paid to surface waves in seismic exploration, where the surface wave is viewed as undesirable noise that affects the imaging of subsurface features.

The objective of the paper is to demonstrate the use of surface wave data acquired as part of a refraction survey for the determination of shallow shear velocity and Q. Even though surface-wave data are available in the distance range of 0 - 40 km, which is much larger than in typical seismic exploration data spreads, the need to process multichannel data is a shared feature. Analysis techniques are reviewed, and are actual data sets are processed.

DATA PROCESSING FOR DISPERSION

Given multichannel data, dispersion information can be obtained by single channel as well as multichannel processing. Single channel processing can provide group velocity dispersion, while multichannel processing is required to obtain phase velocities without making assumptions about source phase or the number of wavelengths between the source and single receiver. The techniques of multiple filter analysis and phase velocity stacking are used to define the dispersion parameters.

Multiple Filter Analysis

Multiple filter analysis was introduced by Dziewonski *et al.* (1969) for the determination of group velocity from a dispersed waveform. Herrmann (1973) studied the use of multiple filter analysis to estimate spectral amplitudes of the various modes. Let the Fourier transform of dispersed propagating wave at distance r be $A(\omega,r)e^{-j(k(\omega)r-\phi)}$. Define a Gaussian filter as

$$H(\omega) = \begin{cases} e^{(-\alpha(\omega-\omega_c)^2/\omega_0^2)} & |\omega-\omega_0| \le \omega_c \\ 0 & |\omega-\omega_0| > \omega_c \end{cases} \quad (1)$$

where

$$\omega_c = \omega_0(\pi/\alpha)^{1/2}$$

The result of applying this filter to a dispersed signal is a filtered time signal whose envelope reaches a maximum at the group velocity arrival times. The envelope of the filtered time history for a single mode is approximately

$$g(t,r) = \frac{A(\omega_0,r)\omega_0}{2\pi}\left(\frac{\pi}{\alpha}\right)^{1/2} e^{(-\omega_0^2(t-r/U_0)^2/4\alpha)} \quad (2)$$

Computationally, the time series is filtered using (1), a Hilbert transform of the filtered time series is taken, and the two are combined to form the envelope. The envelope is searched for the relative maxima, from which the group velocity is computed from the time of the peak amplitude and the spectral amplitude is estimated from (2) by the relation $A(\omega_0,r) = g_{max}(2\pi/\omega_0)(\alpha/\pi)^{1/2}$.

For ease of analysis each two plots are made for each trace analyzed. The first presents the spectral amplitude versus frequency, annotating each with a symbol related to the value of the relative amplitude. The second plot provides contours of the envelope as a function of group velocity and frequency, with the group velocities of the envelope peaks indicated by the same symbol as the first plot. Examination of both plots assists in the identification of modes.

For a given shot, individual traces are processed using multiple filter analysis, and a table containing the frequency, group velocity and spectral amplitude is produced. Assuming a laterally homogeneous waveguide, the individual group velocity estimates of a given mode will be identical, and the decay of spectral amplitude with distance, r, will have a functional form

$$A(\omega,r) = A_0 e^{-\gamma r}\, r^{-1/2}. \quad (3)$$

An interactive program, which works on non-graphic computer displays, is used first to identify the modes on the basis of a group velocity histogram, and then to define the anelastic attenuation coefficient, γ, through a least squares fit of observed spectral amplitude of this mode according to the model (3). Provisions are made for editing extreme outliers. The result of this interactive program is a tabulation of group velocities and anelastic attenuation values together with their standard errors, for use with an inversion program.

Group Velocity Stacking

The above technique for estimating the average group velocity and anelastic attenuation over the profile requires running multiple filter analysis for each trace, consolidation of output into a large file, and then interactively editing the data set.

Barker (1988) introduced the idea of determining the group velocity by stacking the envelopes of different traces for a given frequency. This is possible if the envelopes are transformed from a function of time to a function of group velocity. The group velocity of the spread is obtained by searching for the maximum of the stack. If a program automatically selects the maximum, it can then return to the envelope of each trace to search for the maximum in the neighborhood of the velocities from the automatic selection so that error estimates of the group velocity can be made. In addition, spectral amplitudes can be used to estimate anelastic attenuation coefficients.

Phase Velocity Stacking

McMechan and Yedlin (1981) introduced a technique for the determination of phase velocity by performing a $p-\tau$ stack followed by a transformation into the $p-\omega$ domain. Mokhtar *et al* (1988) described a procedure for accomplishing this by first Fourier transforming the time series, and then performing the stacking operation in the frequency domain. Let the Fourier spectrum of a seismic signal of the i'th station at distance r_i be

$$A(\omega,r_i)e^{j\psi(\omega)_i}, \tag{4}$$

where the phase term $\psi(\omega)$ includes a distant dependent component for propagation. The $p-\omega$ stack of N traces is defined by the relation

$$U(p,\omega)=\sum_{i=1}^{N} C(\omega)^{-1}A(\omega,r_i)e^{j\psi_i}e^{j\omega pr_i}. \tag{5}$$

where

$$C(\omega) = A(\omega,r_1)e^{j\psi_1}.$$

Division by $C(\omega)$ is a simple artifice to normalize the spectrum and remove the source phase if the signal is that of a single mode. The observed spectrum is assumed to be the superposition of M surface-wave modes such that

$$A(\omega,r_i)e^{j\phi_i}=\sum_{k=1}^{M} S_k(\omega,r_i)e^{j[\phi_{0k}(\omega)-\omega p_{0k}(\omega)r_i]}, \tag{6}$$

where $S_k(\omega,r_i)$ is the amplitude spectrum of the k'th mode and the phase is separated into distance-independent, $\phi_{0k}(\omega)$, and distance-dependent, $\omega p_{0k}(\omega)r_i$ components. p_{0k} is the inverse of the phase velocity of the k'th mode at frequency ω.

If the signal consists primarily of a single noise free surface-wave mode at a given frequency, then the quantity $U(p,\omega)$ will have a maximum when $p = p_{0k}$. Alternatively it is convenient to search for the maximum of the function

$$|\,U(p,\omega)\,| \tag{7}$$

to find the dispersion curves since it is a real function. Since there are N distances, the maximum value of the quantity $|U(p,\omega)|$ should be equal to N.

If this value is less than N, then we may attribute this to an error in the ray parameter between the stations and thus estimate the error in the corresponding phase velocity. If we assume that in the neighborhood of a stack maximum the quantity $\Delta p = p - p_{0k}$ has a normal distribution with zero mean and a variance σ^2, then the expected value of any term in (4) is

$$E[e^{-j2\pi f \Delta p r_i}] = e^{-2\sigma^2\pi^2 f^2 r_i^2} \tag{8}$$

where we used the definition $\omega = 2\pi f$.

Since each term in (7) is always positive, the expected value of the stack (5) of a single mode is just

$$\left| \sum_{i=1}^{N} e^{-2\sigma^2\pi^2 f^2 (r_i - r_1)^2} \right| \tag{9}$$

Given the stack value (7), a Newton-Raphson technique is used to find the value of σ from (9) that corresponds to this value. The error in phase velocity is obtained using the definition $c = 1/p$ and the relation

$$\Delta c = \sigma c^2. \tag{10}$$

This relation was tested by numerically modeling a stacking operation in which the ray parameter error had the assumed distribution.

In the more realistic case of multimode surface waves, (7) will not yield a maximum independent of the amplitude spectrum of the other modes. Thus the stack value at a given frequency will typically be largest for one mode and smaller for others. The simplistic error analysis will yield larger, perhaps unwarranted, errors for the other modes. This is an inherent problem with this technique, that can only be resolved if a phase matched filter technique is first applied to each input spectra to isolate a single mode before the phase velocity stack is performed.

Evaluation of Techniques

All these techniques suffer from the need for manual intervention to correctly define the dispersion data, especially identification of the mode. The only real identification of the mode number is to count the zero crossings of the surface-wave eigenfunctions, with the fundamental mode Love and vertical component Rayleigh eigenfunctions having zero zero-crossings with depth. Eigenfunction-depth data are not available with surface sensors. An alternative technique uses the fact that the fundamental mode has the lowest phase, and usually group, velocities at any frequency. For surface sources, the fundamental mode is often the one with largest amplitudes.

The fact that the spectral amplitude level of the surface wave modes varies with frequency, the source excitation forces, and with distance due to anelastic attenuation, means that not necessarily the same mode is dominant at a given frequency. Because of this, the phase velocity stacking and multiple filter techniques will find it difficult to follow the dispersion curves of a low amplitude mode in the presence of a larger amplitude.

The group velocity stacking technique works reasonably well for estimating

the group velocity value, even though the determination of the average group velocity should be weighted as a function of distance, since the group velocity resolution is less at shorter distances. The automatic determination of the anelastic attenuation coefficient, γ, also requires such a weighting. In addition, since this depends upon spectral amplitude estimates, the interference of modes at short distances will give erroneously spectral amplitudes, and thus overestimate the γ values. In such a case, it is better to run the multiple filter analysis on each individual trace, and then interactively determine the values.

SURFACE WAVE INVERSION

Surface wave inversion is relatively straight forward once the dispersion is correctly defined. This requires a linearization of the problem and the subsequent iterative inversion of the observations.

Love-Wave or SH Formulation.

Following Keilis-Borok *et al.* (1989), the equation for the SH-wave eigenfunction, $V^{(3)}$, in a cylindrical coordinate system is

$$\frac{d}{dz}\begin{bmatrix} V^{(3)} \\ p_{\phi z} \end{bmatrix} = \begin{bmatrix} 0 & 1/\mu \\ \mu k^2 - \rho\omega^2 & 0 \end{bmatrix}\begin{bmatrix} V^{(3)} \\ p_{\phi z} \end{bmatrix}, \tag{11}$$

where k is the wavenumber, ω is the angular frequency, μ is the rigidity and ρ is density. The boundary conditions for surface waves are that $p_{\phi z}(z=0) = 0$, and $V^{(3)}(z) \to 0$, as $z \to \infty$.

A discrete solution to the boundary conditions satisfies the equation

$$\begin{aligned} L &= \omega^2 I_0 - k^2 I_1 - I_2 \\ &= \omega^2 \int_0^\infty \rho (V^{(3)})^2 dz - k^2 \int_0^\infty \mu (V^{(3)})^2 dz - \int_0^\infty \mu \left(\frac{dV^{(3)}}{dz} \right)^2 dz , \end{aligned} \tag{12}$$

where L is the Lagrangian. The group velocity is determined from the relation

$$U = \frac{d\omega}{dk} = kI_1/\omega I_0 . \tag{13}$$

If the medium is split into constant velocity-density layers, of thickness d_m, density ρ_m, and shear-wave velocity β_m, and the layer is bounded by $z = z_m - d_m$ and $z = z_m$, then the partials of the phase velocity with shear velocity for fixed frequency and density, and with density for fixed frequency and shear-wave velocity are

$$\left(\frac{\partial c}{\partial \beta} \right)_m = \frac{\beta_m \rho_m}{UI_0} \int_{z=z_m-d_m}^{z_m} \left[(V^{(3)})^2 + \left(\frac{1}{k} \frac{dV^{(3)}}{dz} \right)^2 \right] dz \tag{14}$$

and

$$\left(\frac{\partial c}{\partial \rho} \right)_m = \frac{\beta_m}{2\rho_m} \left(\frac{\partial c}{\partial \beta} \right)_m - \frac{c^2}{2UI_0} \int_{z=z_m-d_m}^{z_m} (V^{(3)})^2 dz . \tag{15}$$

Rayleigh Wave of P-SV Formulation

In a cylindrical coordinate system, the equation of motion governing the eigenfunctions is

$$\frac{d}{dz}\begin{bmatrix} V^{(1)} \\ V^{(2)} \\ p_{zz} \\ p_{rz} \end{bmatrix} = \begin{bmatrix} 0 & k\lambda/(\lambda+2\mu) & 1/(\lambda+2\mu) & 0 \\ -k & 0 & 0 & 1/\mu \\ -\rho\omega^2 & 0 & 0 & k \\ 0 & -\rho\omega^2+4k^2\mu(\lambda+\mu)/(\lambda+2\mu) & -k\lambda/(\lambda+2\mu) & 0 \end{bmatrix} \begin{bmatrix} V^{(1)} \\ V^{(2)} \\ p_{zz} \\ p_{rz} \end{bmatrix} \quad (16)$$

where the vertical component eigenfunction is $V^{(1)}$, and the radial component eigenfunction is $V^{(2)}$. The ellipticity at the free surface is $\epsilon = V^{(2)}(0)/V^{(1)}(0)$. The boundary conditions for surface waves are that $p_{rz}(z=0) = 0$, $p_{zz}(z=0) = 0$, $V^{(1)}(z) \to 0$, as $z \to \infty$. and $V^{(2)}(z) \to 0$, as $z \to \infty$.

A discrete solution to the boundary conditions satisfies the equation

$$L = \omega^2 I_0 - k^2 I_1 - 2kI_2 - I_3 , \quad (17)$$

where L is the Lagrangian, and

$$I_0 = \int_0^\infty \rho \left[(V^{(1)})^2 + (V^{(2)})^2 \right] dz \quad (18)$$

$$I_1 = \int_0^\infty \left[\mu (V^{(1)})^2 + (\lambda+2\mu)(V^{(2)})^2 \right] dz \quad (19)$$

$$I_2 = \int_0^\infty \left[\mu V^{(1)} \frac{dV^{(2)}}{dz} - \lambda V^{(2)} \frac{dV^{(1)}}{dz} \right] dz \quad (20)$$

$$I_3 = \int_0^\infty \left[(\lambda+2\mu) \left(\frac{dV^{(1)}}{dz} \right)^2 + (\mu) \left(\frac{dV^{(2)}}{dz} \right)^2 \right] dz . \quad (21)$$

The group velocity is determined from the relation

$$U = \frac{d\omega}{dk} = (kI_1 + I_2)/\omega I_0 . \quad (22)$$

If the medium is split into constant velocity-density layers, of thickness d_m, density ρ_m, compressional-wave velocity α_m, and shear-wave velocity β_m, and the layer is bounded by $z = z_m - d_m$ and $z = z_m$, then the partials of the phase velocity with shear velocity for fixed frequency, compressional velocity and density, with compressional velocity for fixed frequency, shear velocity and density, and with density for fixed frequency and compressional and shear velocity are

$$\left(\frac{\partial c}{\partial \alpha} \right)_m = \left(\frac{\alpha_m \rho_m}{U I_0} \right) \int_{z=z_m-d_m}^{z_m} \left[V^{(2)} - \frac{1}{k} \frac{dV^{(1)}}{dz} \right]^2 dz \quad (23)$$

$$\left(\frac{\partial c}{\partial \beta}\right)_m = \left(\frac{\beta_m \rho_m}{UI_0}\right) \int_{z=z_m-d_m}^{z_m} \left[\left(V^{(1)} + \frac{1}{k}\frac{dV^{(2)}}{dz}\right)^2 + \frac{4}{k}V^{(2)}\frac{dV^{(1)}}{dz}\right] dz \tag{24}$$

$$\left(\frac{\partial c}{\partial \rho}\right)_m = \frac{1}{2\rho}\left[\alpha\left(\frac{\partial c}{\partial \alpha}\right)_m + \beta\left(\frac{\partial c}{\partial \beta}\right)_m\right] - \frac{c^2}{2UI_0}\int_{z=z_m-d_m}^{z_m}\left[(V^{(1)})^2 + (V^{(2)})^2\right] dz \ . \tag{25}$$

If the material properties within each layer are constant, propagator techniques can be used to determine the dispersion and eigenfunctions and the integrals can be analytically evaluated (Harkrider, 1979; Wang, 1981).

Numerical Partial Derivation Computaiton and Causality

The partial of group velocity with respect to a layer parameter v is

$$\frac{\partial U_o}{\partial v} = \frac{U_o}{c_o}\frac{\partial c_o}{\partial v} + \frac{U_o^2}{c_o^2}\left(\frac{T}{c}\frac{dc_o}{dt}\frac{\partial c_o}{\partial v} - T\frac{\partial}{\partial T}\frac{\partial c_o}{\partial v}\right) \tag{26}$$

The phase velocity partial with respect to period is *numerically* computed using the relation

$$\frac{\partial}{\partial T}\frac{\partial c_o}{\partial v} = T\left[\left(\frac{\partial c_o}{\partial v}\right)_{T+hT} - \left(\frac{\partial c_o}{\partial v}\right)_{T-hT} / 2hT\right]$$

In these expressions, the parameter v can take on the values α, β or ρ, and the subscript o represents the value in the parameter in the purely elastic model.

If a causal Q is introduced, a Futterman causality tied to a reference angular frequency ω_r, the elastic parameters will equal the anelastic values when the angular frequency ω equals ω_r. The causal phase velocity c is given by

$$c = c_o + \frac{1}{\pi}\ln\left(\frac{\omega}{\omega_r}\right)\sum\left(\frac{\partial c_o}{\partial \beta}\beta Q_\beta^{-1} + \frac{\partial c_o}{\partial \alpha}\alpha Q_\alpha^{-1}\right) \tag{27}$$

and the value of the spatial anelastic attenuation factor, γ, is

$$\gamma = \frac{\omega}{2c_o^2}\sum\left(\frac{\partial c_o}{\partial \beta}\beta Q_\beta^{-1} + \frac{\partial c_o}{\partial \alpha}\alpha Q_\alpha^{-1}\right) \tag{28}$$

In order to obtain the correct partial derivatives of causal phase velocity and gamma with respect to the model parameters, the following are used. A partial or a parameter without the subscript o represents the causal value. Note that it is assumed that Q_β/Q_α is a fixed ratio, hence a partial with respect to Q_β^{-1} may involve a partial of c_o with respect to α.

$$\frac{\partial c}{\partial v} = \frac{\partial c_o}{\partial v}\left(1 + \frac{1}{\pi Q_v}\ln\left(\frac{\omega}{\omega_r}\right)\right) \tag{29}$$

$$\frac{\partial c}{\partial Q_\beta^{-1}} = \frac{1}{\pi}\ln\left(\frac{\omega}{\omega_r}\right)\left(\frac{\partial c_o}{\partial \beta}\beta + \frac{\partial c_o}{\partial \alpha}\alpha\frac{Q_\beta}{Q_\alpha}\right) \tag{30}$$

$$\frac{\partial \gamma_i}{\partial v} = \frac{\omega}{2c_o^2}\frac{\partial c_o}{\partial v}Q_\beta^{-1} - 2\frac{\gamma}{c_o}\frac{\partial c_o}{\partial v} \tag{31}$$

$$\frac{\partial \gamma_i}{\partial Q_\beta^{-1}} = \frac{\omega}{2c_o^2}\left(\frac{\partial c_o}{\partial \beta}\beta + \frac{\partial c_o}{\partial \alpha}\alpha\frac{Q_\beta}{Q_\alpha}\right) \tag{32}$$

$$U = U_o\left(1 + (2-\frac{U_o}{c_o})\left(\frac{c-c_o}{c_o}\right) + \frac{2\gamma U_o}{\pi\omega}\right). \tag{33}$$

where it is assumed in the derivation that $\left(\frac{c-c_o}{c_o}\right)^2$ is negligible.

$$\frac{\partial U}{\partial v} = \frac{\partial U_o}{\partial v}\left(\frac{U}{U_o} - \frac{U_o}{c_o}\left(\frac{c-c_o}{c_o}\right) + \frac{2\gamma U_o}{\pi\omega}\right) \tag{34}$$
$$+ \frac{\partial c_o}{\partial v}\frac{U_o}{c_o}\left(-2\frac{2\gamma U_o}{\pi\omega} + \frac{U_o}{c_o}\frac{1}{\pi Q_v}\right.$$
$$\left. + (2-\frac{U_o}{c_o})(\frac{1}{\pi Q_v}\ln(\frac{\omega}{\omega_r}) - \left(\frac{c-c_o}{c_o}\right))\right)$$
$$+ \frac{U_o^2}{c_o^2}\left(\frac{c-c_o}{c_o}\right)\frac{\partial c_o}{\partial v}$$

$$\frac{\partial U}{\partial Q_\beta^{-1}} = \frac{U_o}{c_o}(2-\frac{U_o}{c_o})\frac{\partial c}{\partial Q_\beta^{-1}} \tag{35}$$
$$+ \frac{1}{\pi}\frac{U_o^2}{c_o^2}(\frac{\partial c_o}{\partial \beta}\beta + \frac{\partial c_o}{\partial \alpha}\alpha\frac{Q_\beta}{Q_\alpha})$$

An iterative linear inversion is performed because of the non-linear nature of the problem. At any stage there is a current model which is used to predict the observations and there is also a lack of fit. For simplicity, the compressional wave velocity α is not directly inverted, rather it is tied to the shear velocity by an *a priori* assumption, such as a constraint that constant Poisson's ratio be constant. We may thus express the difference between observed and predicted values as a linear function of changes in shear velocity model and changes in the inverse Q model. Since the effect of compressional wave Q_α may not be negligible, the compressional wave Q_α is related to the shear wave Q_β by a ratio Q_α/Q_β for the layers. Given these assumptions, the inversion can take on two appearances, non-causal and causal, depending upon which partial derivatives are used. To keep the notation general, the partial derivatives with respect to layer velocity in the next three equations can either be causal or non-causal.

The differences in observed and predicted phase velocities are modeled as

$$c_{obs} - c_{pred} = \frac{\partial c}{\partial \beta_1}\Delta\beta_1 + \cdots + \frac{\partial c}{\partial \beta_n}\Delta\beta_n + \frac{\partial c}{\partial Q_{\beta_1}^{-1}}\Delta Q_{\beta_1}^{-1} + \cdots + \frac{\partial c}{\partial Q_{\beta_n}^{-1}}\Delta Q_{\beta_n}^{-1}, \tag{36}$$

the difference between observed and predicted group velocities is given by

$$U_{obs} - U_{pred} = \frac{\partial U}{\partial \beta_1}\Delta\beta_1 + \cdots + \frac{\partial U}{\partial \beta_n}\Delta\beta_n + \frac{\partial U}{\partial Q_{\beta_1}^{-1}}\Delta Q_{\beta_1}^{-1} + \cdots + \frac{\partial U}{\partial Q_{\beta_n}^{-1}}\Delta Q_{\beta_n}^{-1} \quad (37)$$

and the difference between observed and gamma values predicted by the current model is

$$\gamma_{obs} - \gamma_{pred} = \frac{\partial \gamma}{\partial \beta_1}\Delta\beta_1 + \cdots + \frac{\partial \gamma}{\partial \beta_n}\Delta\beta_n + \frac{\partial \gamma}{\partial Q_{\beta_1}^{-1}}\Delta Q_{\beta_1}^{-1} + \cdots + \frac{\partial \gamma}{\partial Q_{\beta_n}^{-1}}\Delta Q_{\beta_n}^{-1} \quad . \quad (38)$$

Once set up, the system of linear equations is solved using singular value decomposition (Russell, 1987). Provisions are made to damp the solutions as a mean of controlling convergence. Inversion can be performed in an unweighted manner, or can be perform using *a priori* weights available from the error estimates from the dispersion analysis. In addition, a differential inverse can be use to solve for the change in inversion parameter across a layer boundary, rather than for the parameter itself. This constraint guarantees a smooth model and avoids unrealistic alternating low velocity layers in the resulting model.

MAINE REFRACTION EXPERIMENT

In 1984, the U. S. Geological Survey ran a series of refraction experiments in the state of Maine (Murphy and Luetgert, 1986; Murphy and Luetgert, 1987). The refraction profiles went both along (NE) and cross (NW) the strike of the Appalachian Mountains. Surface geology varied significantly in lithology and geologic age. Because of the excellent data set, both in spatial sampling and calibrated instruments, this data set was analyzed to learn about shallow shear-wave velocity and Q.

Figure 1 shows the data from one shot point, SP1 with distance increasing in a southeast direction. Fundamental mode phase velocity and spatial attenuation values were inverted, with the resulting earth model given in Table 1. To avoid any bias of the initial model upon the inverted model, the inversion started with a twelve layered model with velocities and densities of each layer equal to that of the halfspace. The inferred velocities in the lower part of the model are not well resolved. The high values are not unexpected given the highly metamorphosed geology sampled by the surface waves.

Figure 2 presents the fundamental mode synthetic seismograms for an explosion source in this model. The arrival times and waveforms compare well to the observed data of Figure 1. As a check on the correctness of the inversion, both the synthetic and observed data were filtered through the same narrow band band-pass filters, and the peak amplitudes plotted as a function of distance. This exercise showed that the derived Q_β model explained the observed decrease of amplitude with distance.

FUTURE DIRECTIONS

Experience with limited data sets indicate certain rules for estimating the depth limits of surface-wave inversion. Since longer periods or longer

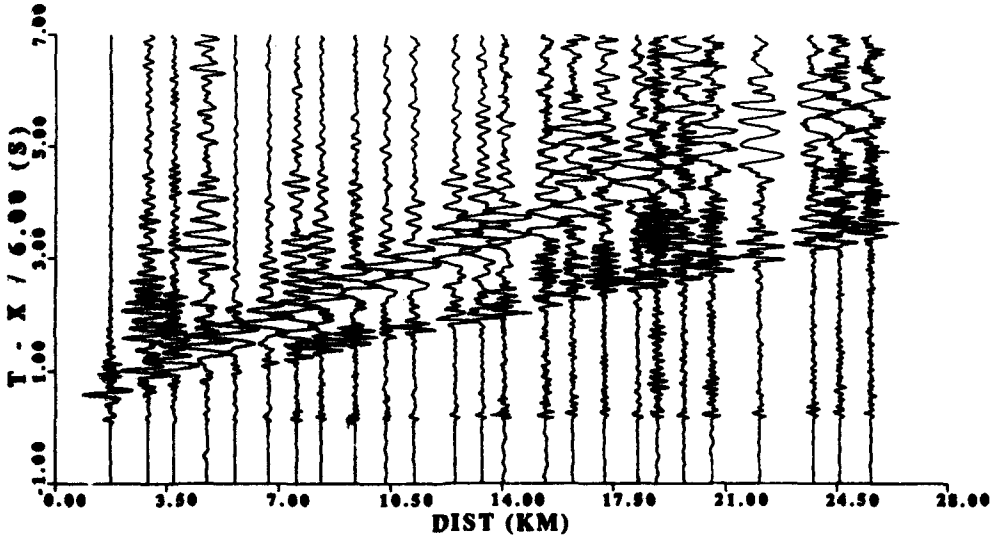

Figure 1. Data for SP1, plotted using a reduction velocity of 6.0 km/s. The data have been low pass filtered between 0.5 and 5.0 Hz.

TABLE 1. Velocity Model for SP1

H (km)	α (km/s)	β (km/s)	ρ (g/cm^3)	Q_α	Q_β
0.25	4.45	2.57	2.37	64	32
0.25	5.61	3.24	2.62	64	32
0.25	5.85	3.38	2.67	64	32
0.25	6.15	3.55	2.74	70	35
0.25	6.30	3.64	2.79	74	37
0.25	6.40	3.70	2.82	84	42
0.25	6.41	3.70	2.82	96	48
0.25	6.44	3.72	2.83	114	57
0.50	6.45	3.72	2.83	142	71
0.50	6.49	3.75	2.85	190	95
0.50	6.50	3.76	2.85	284	142
	6.65	3.84	2.89	568	284

wavelength surface waves penetrate deeper, and since longer periods are better resolved at larger distances, two such rules are 1) the surface wave provides resolvable information to depths on the order of 1/3 – 1 λ, where λ is

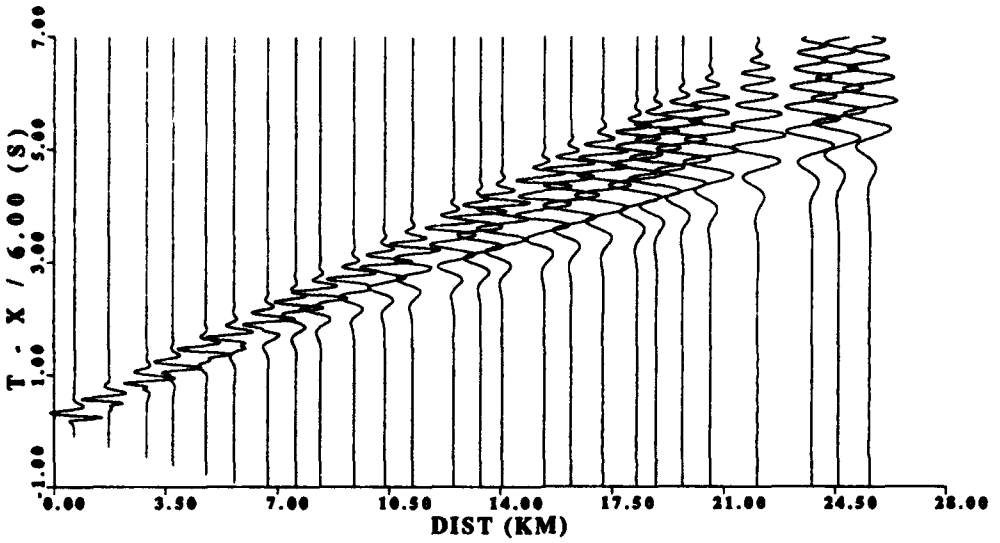

Figure 2. Synthetic traces for SP1, plotted using a reduction velocity of 6.0 km/s. The data have been low pass filtered between 0.5 and 5.0 Hz and also passed through a 2 Hz seismometer for proper comparison with Figure 1.

the longest observed wavelength, and 2) the maximum depth is on the order of 1/20 – 1/10 r_{max}, where r_{max} is the of the maximum distance of observation. This relatively limited depth resolution, compared to refraction analysis, is mitigated by the ability to resolve changes in the surface-wave waveguide within a given shot spread.

The data sets analyzed and the inversion programs developed both considered land based data. Introduction of a water layer is simple, and is already encompassed in the theory presented. There is no difficulty in using surface-wave inversion techniques for data acquired in shallow marine sediments.

ACKNOWLEDGMENTS

The assistance of W. Kohler and W. Mooney of the USGS in providing the data set is appreciated.

REFERENCES

Barker, T. (1988). Array processing of Rayleigh waves for shallow shear wave velocity structure (abs), *Seismological Research Letters* 59, 12.

Dziewonski, A. M., S. Bloch, and M. Landisman (1969). A technique for the analysis of transient seismic signals, *Bull. Seism. Soc. Am.* 59, 427-444.

Ewing, W. M., W. S. Jardetzky, and F. Press (1957). *Elastic Waves in Layered Media*, McGraw Hill, Inc., New York.

Harkrider, D. G. (1979). Eigenfunction normalization for energy calculations in surface wave codes (abs), Earthquake Notes 50, No. 4, 28.

Herrmann, R. B. (1973). Some aspects of band-pass filtering of surface waves, *Bull. Seism. Soc. Am.* 63, 663-671.

Kolla-Borok, V. L., A. L. Levshin, T. B. Yanovskaya, A. V. Lander, B. G. Bukchin, M. P. Barmin, L. I. Ratnikova, and E. N. Its (1989). *Seismic surface waves in a laterally inhomogeneous earth*, Kluwer Academic Publishers, Dordrecht.

McMechan, G. A. and M. J. Yedlin (1981). Analysis of dispersive waves by wave field transformation, *Geophysics* 46, 869-874.

Mokhtar, T. A., R. B. Herrmann and D. R. Russell (1988). Seismic velocity and Q model for the shallow structure of the Arabian shield from short-period Rayleigh waves, *Geophysics* 53, 1379-1387.

Murphy, J. M. and J. H. Luetgert (1986). Data report for the Maine-Quebec cross-strike seismic-refraction profile, *U. S. Geological Survey Open-File Report 86-47*, Menlo Park, CA.

Murphy, J. M. and J. H. Luetgert (1987). Data report for the Maine along-strike seismic-refraction profiles, *U. S. Geological Survey Open-File Report 87-133*, Menlo Park, CA.

Nolet, G. (1987). Waveform Tomography, in *Seismic Tomography*, edited by G. Nolet, pp 301-322, D. Reidel, Hingham, Mass.

Nolet, G. (1990). Partitioned waveform inversion and two-dimensional structure under the network of autonomously recording seismographs, *J. Geophys. Res.* 95, 8499-8512.

Russell, D. R. (1987). Multichannel processing of dispersed surface waves, *Ph. D. Dissertation*, Saint Louis University.

Wang, C. Y. (1981). Wave theory for seismogram synthesis, *Ph. D. Dissertation*, Saint Louis University, St. Louis, Missouri.

GROUND-ROLL: A POTENTIAL TOOL FOR CONSTRAINING SHEAR-WAVE STATICS

G. I. Al-Eqabi and R. B. Herrmann

Department of Earth and Atmospheric Sciences,
Saint Louis University,
3507 Laclede, St. Louis, MO 63103.

ABSTRACT

The objective of this study is to demonstrate that a laterally varying shallow shear-wave structure, derived from the dispersion of the ground roll, can explain observed lateral variations in the direct shear-wave arrival, which occur at same places where ground-roll moveout changes. The data set consists of multichannel seismic refraction data from a USGS-GSC survey in the state of Maine and the Province of Quebec. These data exhibit significant lateral changes in the moveout of the ground-roll as well as the S-wave first arrivals. A sequence of surface-wave processing steps are used to obtain a final laterally varying shear-wave velocity model. These steps include visual examination of the the data, stacking, waveform inversion of selected traces, phase velocity adjustment by cross-correlation, and phase velocity inversion. These models are used to predict the S-wave first arrival by using 2-D ray tracing techniques. Observed and calculated S-wave arrival match well over 30 km long data paths, where lateral variations in the shear-wave velocity in the upper 1-2 km is as much as $\pm 8\%$. The modeled correlation between the lateral variations in the ground-roll and S-wave arrival demonstrates that the problem of shear-wave statics in exploration seismology could be posed as problem of surface-wave propagation.

INTRODUCTION

The observed quality of seismic signals can be degraded by their propagation through shallow-inhomogeneities and lateral variations in the earth's near-surface structure. Near-surface structure introduces delays in the recorded travel times which can cause signal misalignment that distorts the apparent earth structure and stratigraphy (Wiggins et al, 1976; Rothman, 1986). Since near-surface time anomalies can have an adverse effect on all subsequent processing and interpretation of seismic data, an independent constraint on the shallow shear-wave velocity could improve the seismic exploration results. Usually this is done by a statics analysis applied to the S-wave first arrivals. Another possibility is to make use of the ground roll, or surface wave, to define a shallow shear-wave velocity model.

It is well known from earthquake seismology that the inversion of surface-wave dispersion can be used to define a shear-wave velocity structure. One can use either Love or Rayleigh wave fundamental and higher mode dispersion. Because of the large distances between seismograph stations in earthquake seismology, inverted earth models represent path averages between seismograph stations and the inverted model thickness is

usually significantly less than the station separation. Mari (1984) used Love wave dispersion to determine static corrections. He used all the traces in the shot spread to define a dispersion curve and corresponding velocity model averaged over the spread length. For purpose of static corrections, the velocity model for each shot spread was assigned to a horizontal position at the center of the spread. Thus a spatially smoothed statics model is derived. In order to improve the static correction, less spatial averaging is required. Efforts have been made in this direction. Nolet (1990) combined waveform modeling techniques with a partitioned inversion scheme to trace lateral variations in earth model beneath a NARS experiment in Europe. His technique is valid for small lateral variations in velocity model.

A refraction survey in the state of Maine conducted by the U. S. Geological Survey and the Geological Survey of Canada crossed complex geological structure that yielded observable lateral variation in the moveout of the P- and S-wave first arrivals and also the surface wave. These data provide an opportunity to see if it is possible to use data from a single shot spread to define a laterally varying, shallow shear-wave velocity model from the surface-wave dispersion and then to see if this velocity model can explain the observed lateral variation in the shear-wave first arrivals.

DATA AND ANALYSIS

Data Set

Murphy and Luetgert (1986, 1987) describe the experiment and data acquisition. Scientific results are given in Klemperer and Luetgert (1987) and Luetgert et al (1989). For our paper, two data sets were chosen: one from shot SP4 in a southeast direction, which is denoted SP4-POS, since it is in the direction of SP5, and the other from SP1 in a northwest direction, which we denote as SP1-NEG. Figure 1 shows the shots and the trend of the recording positions from them.

Data Processing

Figure 2 presents the observed and modeled data for the SP4-POS spread. The vertical component time histories are available at approximately 1 km spacings and are used out to 34 km for this study. The traces are low pass filtered at 5.0 Hz with a two-pole Butterworth causal filter to emphasize the surface wave. A reduction velocity of 3.5 km/s is used to focus attention on the S-wave first arrival. It is obvious that there are lateral changes in the moveout of the S-wave first arrival and closer inspection shows that this is also true for the surface-wave arrival, the fundamental mode Rayleigh wave. To focus on the surface wave arrival, these same data are plotted in Figure 3a with a reduction velocity of 2.5 km/s. The lateral variations in the surface-wave moveout are apparent.

To define the surface-wave dispersion where there is no evidence of lateral variation in the dispersion, one can process the data with a p-ω stack (McMechan and Yedlin, 1981). This will lead to a dispersion curve that can be inverted for an earth model. When there are sharp changes in the waveguide, the p-ω stack may yield two dispersion curves (Mokhtar et al,

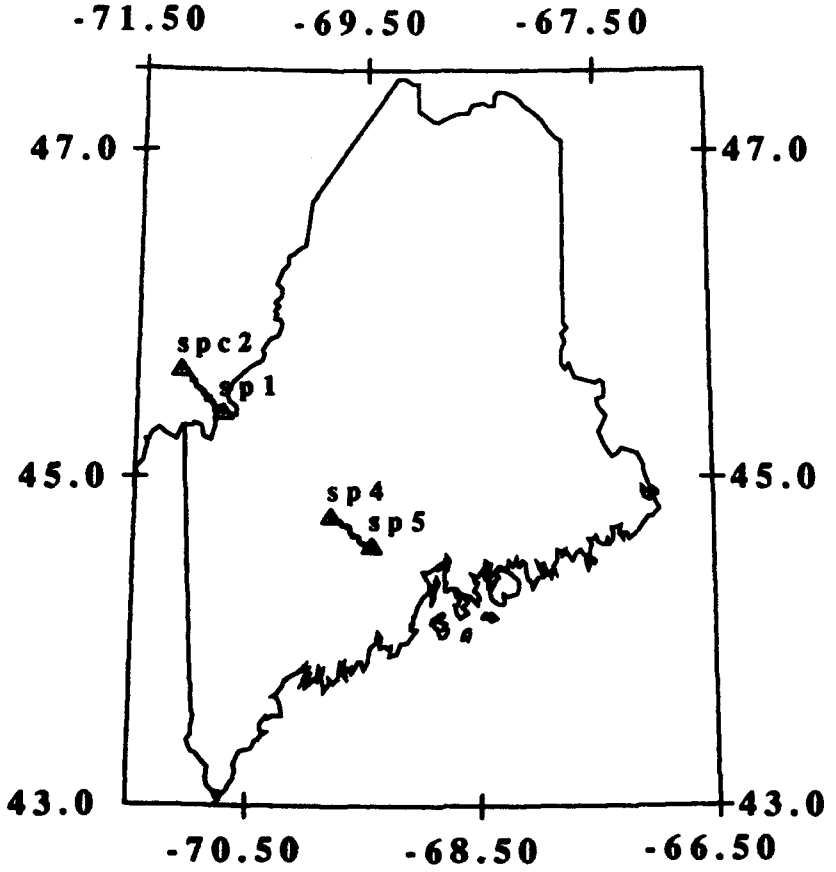

Fig. 1. Map of the study region, showing the shot points, SP1 and SP4, and the data spreads from these shot points.

1988). If the changes are gradual the p-ω stack dispersion curves will be less well defined and an average dispersion curve can be inverted for a first order earth model which can then be used to define an average phase-velocity dispersion curve for the next processing step.

If the signal is assumed to consist only of a fundamental-mode surface wave, then the signal can be analytically dispersed to another distance by a simple frequency domain operator. Let the observed signal at distance r and frequency f be $S(r,f)$. Also let the wavenumber and anelastic attenuation coefficients be defined by $k(f)$ and $\gamma(f)$. Then the signal to be expected at a distance r_1 is

$$S(r_1,f) = S(r,f)(r/r_1)^{1/2} e^{-ik(f)(r_1-r)} e^{-\gamma(f)(r_1-r)} \qquad (1)$$

If the predicted time history at distance r_1 is plotted at r, then any variation in the waveform would represent a violation of the assumptions of wave propagation in a laterally uniform medium and of knowing the true phase velocity dispersion. Figure 3b shows the result of applying such an operation to the traces of Figure 3a when a reference distance r_1 = 30 km is used. Since

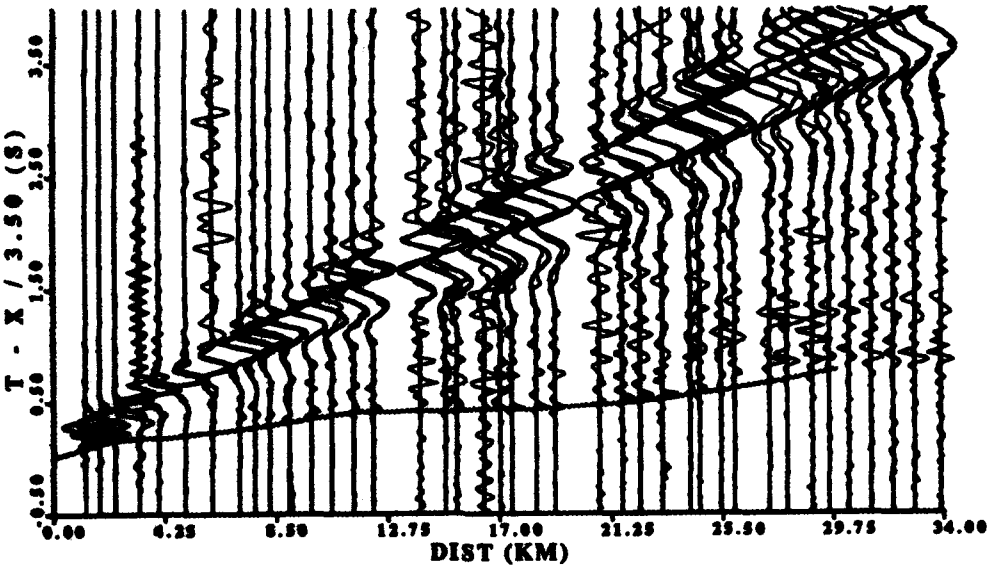

Fig. 2. Observed (light) and predicted (heavy) seismograms of the SP4-POS profile. Both traces have been bandpass filtered between 0.5 - 5.0 Hz. The predicted S-wave arrival times are indicated by the shaded curve.

the first order effects of dispersion have been equalized, the waveforms are similar. Differences at short distances are due to lack of separation of the surface-wave from the rest of the signal in the original data. At large distances, high frequency noise is introduced because the attenuation operator must reintroduce high frequencies to the signal in equalizing the signal to the shorter reference distance. Since the pulse shapes are relatively independent of distance, the first order effects of dispersion have been accounted for. Figure 3b can be viewed as like the reduced travel time plot of refraction seismology, where relative offsets of arrivals represent faster or slower arrivals. It is obvious from Figure 3b, and also from Figure 3a, that there are changes in the surface-wave moveout at about 12, 20 and 27 km from the source. By comparing receiver locations to geological maps, these changes were found to correlate to mapped changes in surface geology.

The initial processing steps are described by Herrmann and Al-Eqabi (1991). Multiple filter analysis is performed on each trace in order to estimate the group velocity and spectral amplitude of the fundamental mode as a function of frequency. The spectral amplitude data are then used to estimate the anelastic attenuation coefficient γ that appears in equation (1). A p-ω stack is performed to obtain phase velocity as a function of frequency. These data can be inverted for shear velocity, β and the shear-wave quality factor,

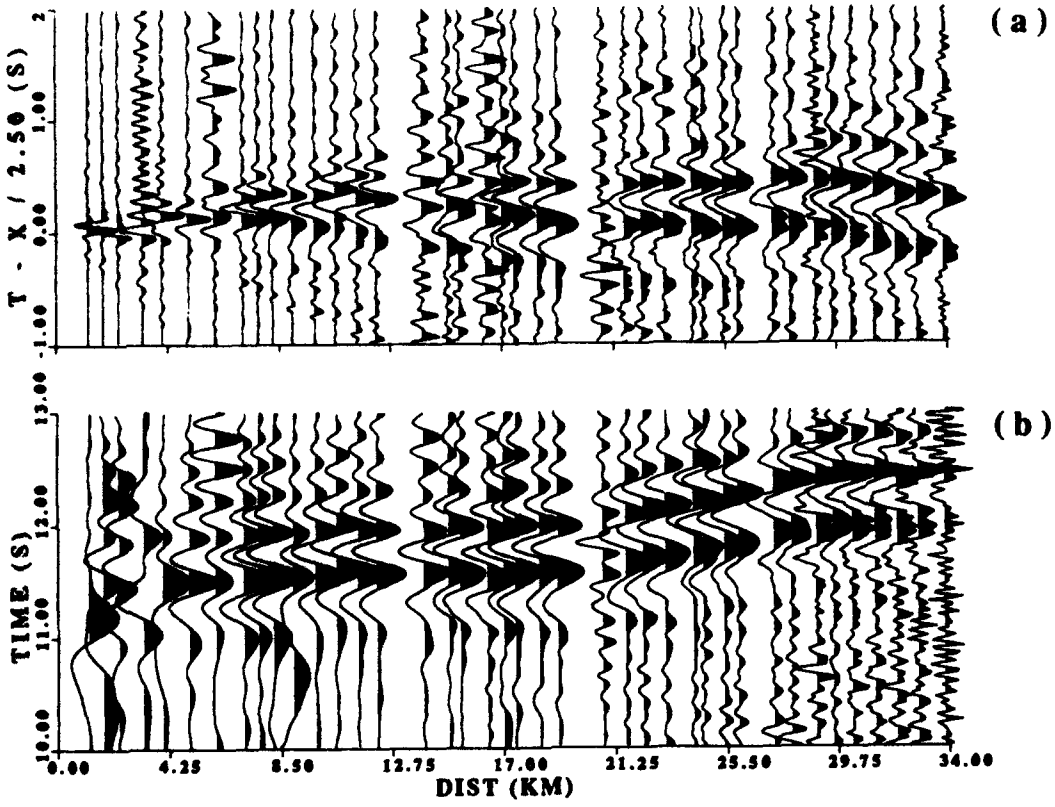

Fig. 3. (a) Filtered observed data of Figure 1, plotted with a reduction velocity of 2.5 km/s to focus on the surface-wave. (b) Traces of Figure 3a equalized for dispersion to a reference distance of 30 km. This display eliminates the distraction of the dispersion in order to focus on the lateral variation apparent in the data set.

Q_β as a function of depth. If lateral variations in dispersion are observed in the data, the spread is partitioned into segments of uniform dispersion, based on an examination of data presentations such as those of Figure 3. Waveform inversion (Nolet, 1990) is applied to the traces at the segment boundaries, and the resultant models are used to generate fundamental mode synthetics, which are then cross correlated using the dispersion curves from the waveform matching models to guide the intertrace phase unwrapping. The result is a dispersion curve specific to each segment. The cross correlation of synthetics rather than actual data traces yields smoother, better behaved intertrace dispersion curves. These dispersion curves are independently inverted to provide the vertical velocity distribution for each segment. Finally synthetic seismograms, including instrument response, are generated for the resultant laterally varying earth model under the assumption of no mode conversion at segment boundaries (Keilis-Borok et al, 1989) and compared to the observed data. A laterally varying model is judged appropriate is the predicted and observed waveforms agree both in shape and level.

Inversions

Table 1 shows the resultant earth model for the SP4 profile. In this table, each segment is defined by the distance of its boundaries from the shot point. A single Q model was assumed for the entire path because of lack of spatial resolution inherent in estimating Q in terms of a spatial decrease in amplitude. In addition, is was assumed that the P-wave velocity, α, is given by $\alpha = 1.732\beta$ and that $Q_\alpha = 2Q_\beta$. Figure 2 compares the observed (light lines) and fundamental mode surface-wave traces (heavy lines) for this data set. Both sets of traces have been bandpass filtered between 0.5 and 5.0 Hz. The agreement is relatively good, except that the surface-wave model does not predict the later reverberations seen in many observed traces.

Table 1. Seven velocity models and Q_β structure
SP4 positive side (SE) obtained from waveform inversion, two Station phase adjustment followed by dispersion inversion.

Segment	1	2	3	4	5	6	7		
Position(km)	0.0-5.0	5.0-11.4	11.4-15.4	15.4-19.1	19.1-21.6	21.6-25.4	25.4-34.3		
H	β	β	β	β	β	β	β	Q_α	Q_β
km	km/sec	km/sec	km/sec	km/sec	km/sec	km/sec	km/sec		
0.250	2.757	2.651	2.651	2.676	2.678	2.458	2.602	60.0	30.0
0.250	3.244	2.996	3.135	3.009	2.514	2.997	2.689	100.0	50.0
0.250	3.309	3.130	3.227	3.132	2.872	3.151	3.110	209.0	104.5
0.250	3.331	3.180	3.220	3.171	3.110	3.186	3.235	366.0	183.0
0.250	3.380	3.232	3.262	3.215	3.172	3.223	3.236	515.0	257.5
0.250	3.415	3.292	3.352	3.268	3.156	3.264	3.247	647.0	323.5
0.250	3.468	3.345	3.456	3.319	3.121	3.294	3.280	784.0	392.0
0.250	3.572	3.381	3.546	3.355	3.105	3.312	3.314	955.0	477.5
0.500	3.572	3.395	3.605	3.370	3.105	3.325	3.332	1202.0	601.0
0.500	3.572	3.395	3.605	3.370	3.120	3.327	3.335	1605.0	802.5
0.500	3.572	3.395	3.605	3.370	3.140	3.323	3.340	2407.0	1203.5
	3.572	3.395	3.605	3.370	3.161	3.317	3.344	4816.0	2408.0

Another way of presenting the results is shown in Figure 4. Here an mean velocity in each layer is obtained and the percentage deviation from the mean in each segment is displayed. A zone of high velocity is seen in the third segment and it is also seen that segments 5-7 have lower surface velocities than segments 1-4.

A question arises as to how much of the resultant velocity model is actually required or even justified. At short distances, little dispersion can be resolved, and there should be less faith in the resultant model. The 4 km thick model was an initial assumption in the inversion, which started with a halfspace model. The dispersion data were permitted to smoothly change the model. However, if the dispersion data could not provide information about deeper structure, that structure was not changed much. While this approach

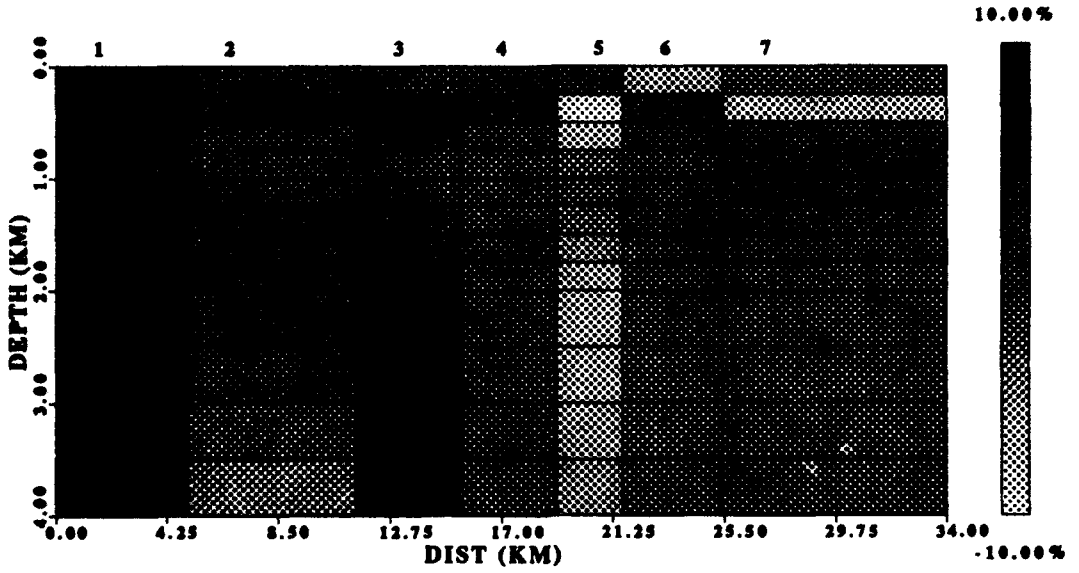

Fig. 4. Representation of lateral varying velocity model for the SP4-POS data set. The shading indicates the percent variation of the layer velocity about the average shear-wave velocity for that layer. The segment number is identified by the name at the top.

might not lead to correct structure at depth, it did permit the data to define a model from an unbiased starting model, e.g., a halfspace, and prevented artificial, inversion induced low velocity zones.

To provide further insight both on depth resolution and also to test the possibility of modeling the S-wave first arrivals, the segmented model was used to predict first arrival times through ray tracing. We used Červený's SEIS81 package to do this. For simplicity the segment model was assumed to represent a single 2-D laterally varying velocity model. The first and last segments were assumed to extend beyond the data range laterally. Horizontal node positions were placed at the midpoints of each segment, and vertical node positions were placed at the midpoints of the first 6 layers, at the surface and at a depth of 3.0 km. The velocity in each layer and segment was assigned to the respective nodes, except that the velocity at the surface equaled that of the top layer of Table 1, and the velocity at a depth of 3.0 km equaled the velocity of layer 8 of Table 1. This latter choice was related to the *ad hoc* experience from surface-wave inversions that the maximum depth resolution is on the order of one-third the longest wavelength resolved or one-tenth to one-twentieth of the spread length.

Figure 5 shows the rays so generated. Their arrival times are plotted in Figure 2 as the shaded curve. It is seen that the predicted S-wave first arrivals match the observed arrivals in time. Recall that the S-wave arrival times were

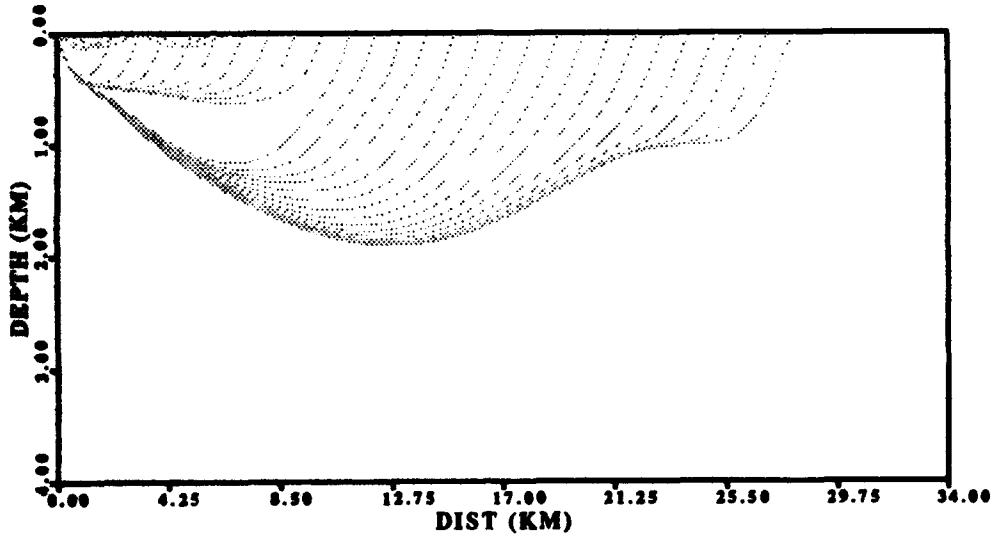

Fig. 5. Result of tracing rays through the velocity model of Table 1.

not used to derive the laterally varying velocity model.

Figure 6 shows the data set from the SP1 spread to the northwest. The shear-wave arrivals are well developed and show lateral variations in first arrival times. The results of the surface-wave inversions are shown in Table 2. The predicted fundamental-mode surface-wave arrivals are also shown in Figure 6. Figure 7 shows the percentage of lateral variation in each layer for this model. Finally Figure 8 shows the rays traced through the model. The predicted S-wave first-arrivals are shown in Figure 6 by the near-horizontal shaded curve.

DISCUSSION

This study focused on the evaluation of the shallow shear-wave velocity structure by using high frequency Rayleigh surface waves recorded as part of a refraction experiment. Laterally varying earth models were required to fit the data. Seven segments were required to explain the lateral variations observed along the SP4-POS (34 km spread) and six segments required for SP1-NEG (32 km spread). The number of the required segments is a function of the geologic complexity and the amount of change in velocity in the horizontal direction. Most of the derived lateral changes correlate strongly with published geologic data, such as the bedrock geological map of Maine (Osberg et al, 1985). Generally, observed variations in velocity within the upper 1 km, range between ±1.2% and ±8.2%. The S-wave first arrivals show significant lateral changes in moveout in the data sets at places where

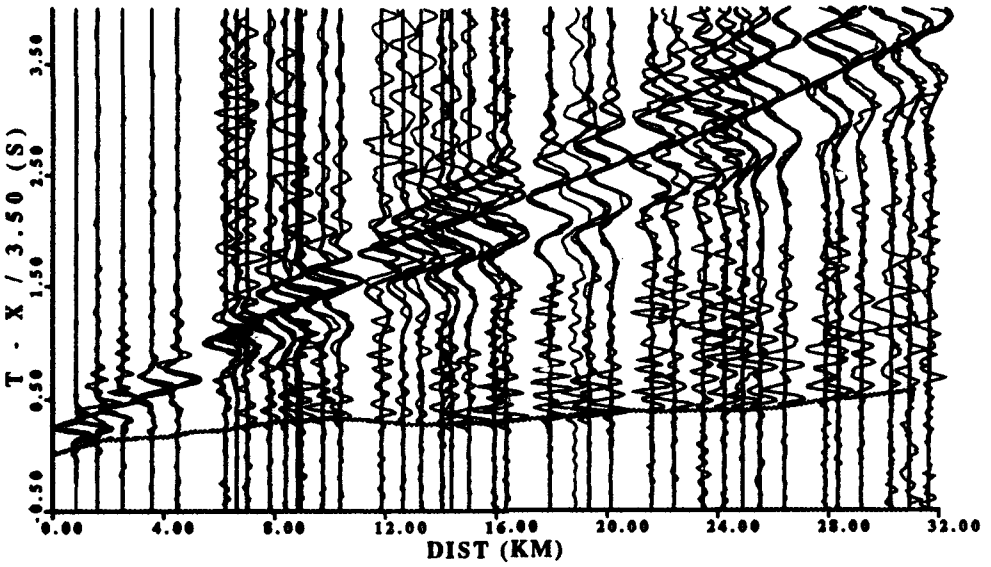

Fig. 6. Observed (light) and predicted (heavy) seismograms of the SP1-NEG profile. Both traces have been bandpass filetered between 0.5 - 5.0 Hz. The predicted S-wave arrival times are indicated by the shaded curve.

strong lateral variations have been observed in the surface wave (Figures 2 and 5). Theoretical S-wave first arrival times, as obtained by 2D ray tracing, show strong correlation with observed S-wave times for the two data set processed.

In the case of the SP4-POS profile we note that Segment 1 has the highest velocity and consists of bands of Upper and Lower Silurian interbedded pelite and limestone and/or dolostone. Segment 2 consists of Devonian-Silurian calcareous sandstones. Segments 3 and 4 have alternating bands of Upper and Lower Silurian interbedded pelite and limestone and/or dolostone. Segments 5 and 6 contain alternating bands of sulfidic pelite, Silurian interbedded pelite and limestone, and Silurian interbedded pelite and sandstone. Finally Segment 7 has Silurian-Ordovician calcareous sandstone. The relatively lower velocities in the upper 0.5 km velocities of segments 6 and 7 seem to correlate with the sandstones. Also note from Figure 4 that Segments 1 and 3 have similar velocity distributions in agreement with the surface geology.

Along the SP1-NEG path, the model not only predicts the direct shear-wave arrival and Rg-wave traces that match the observed traces, but the vertical segment contacts agree with mapped geologic contacts in the area and also with the interpretations drawn from processing reflection data recorded

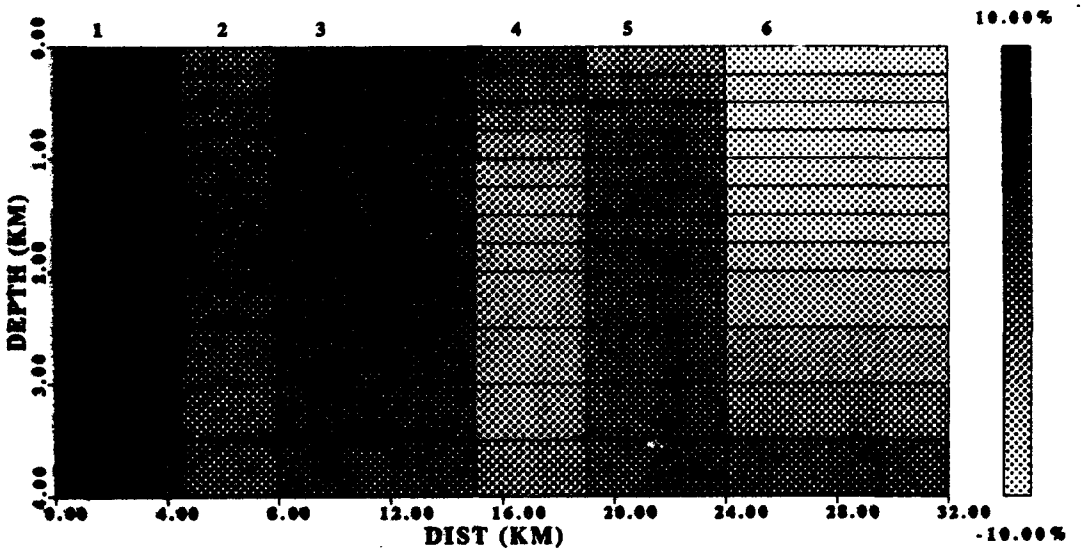

Fig. 7. Representation of lateral varying velocity model for the SP1-NEG data set. The shading indicates the percent variation of the layer velocity about the average shear-wave velocity for that layer. The segment number is identified by the name at the top.

parallel to this path (Luetgert et al, 1989). The boundary between Segments 1 and 2 marks the western boundary of the Chain Lake Massif and the position of the Western boundary Fault. Segment 2 contains Devonian turbidites. The Sandy Stream Fault forms a boundary between Segments 2 and 3. Segment 3 consists of the Clinton and Chesham formations (volcanics, sediments, mélange). Segments 4 and 5 contain the Frontenac formation (terrigenous and volcanic rocks). Finally Segment 6 consists of the highly faulted and folded Silurian and Devonian turbidites of Connecticut Valley - Gaspé Synclinorium and has the lowest velocity within this path. The location of the contacts between Segments 1 and 2 and between Segments 2 and 3 agree with mapped geological contacts and with events C and Y in the Luetgert et al (1989) reflection interpretation.

The ray tracing accomplished two tasks. First, it demonstrated the power of the surface-wave based shear-wave velocity model to predict S-wave first arrivals. Second, it provided some idea of the depth of penetration of the shear-waves. If we assume that the first arriving shear waves penetrate as deep or deeper than the surface waves. This conjecture may be justified by mode-ray duality considerations.

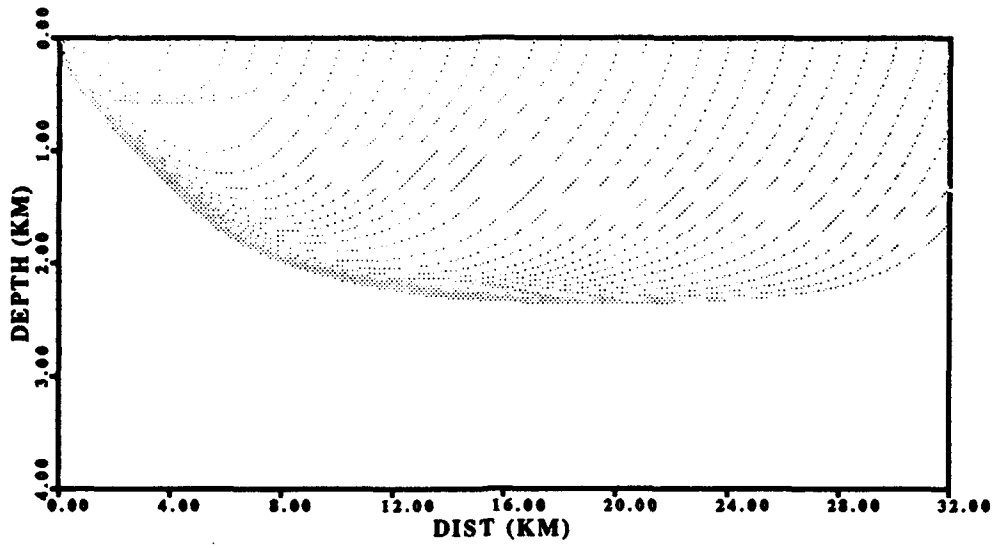

Fig. 8. Result of tracing rays through the velocity model of Table 2.

While the data analysis satisfied the objective of this paper, additional work is required to make this a robust tool for exploration geophysics, especially with respect to shear-wave statics. The primary problem is that many individual steps are required, each of which requires significant data manipulation. If laterally varying phase-velocity dispersion functions can be defined directly from the trace data in a single processing step, then the inversion for the corresponding shear-wave velocity model is relatively trivial. One approach would be to build upon the combination of multi-channel processing and phase match filtering used by Russell (1987) for analyzing dispersion in a laterally homogeneous environment to model the interstation phase delays using a laterally varying phase delay model. Another aspect of processing required to make the results more convenient would be to keep layer velocities fixed and to invert for layer thickness. This would lead to a shallow shear-wave velocity model better related to statics modeling. Keilis-Borok et al (1989) provided the necessary surface-wave perturbation theory to accomplish this. Thus the routine use of the ground roll to constrain shallow shear-wave velocities for use in shear-wave statics estimation is possible.

ACKNOWLEDGMENTS

The assistance of W. Kohler and W. Mooney of the USGS in providing the data set is appreciated. We thank Prof. G. Nolet of the University of the Netherlands for fruitful discussions and for supplying a version of his waveform inversion software.

Table 2. Six velocity models and Q_β structure for SP1 negative side (NW) obtained from waveform inversion, two station phase adjustment followed by dispersion inversion.

Segment	1	2	3	4	5	6		
Position(km)	0.0-4.5	4.5-8.0	8.0-15.0	15.0-19.0	19.0-24.0	24.0-32.0		
H	β	β	β	β	β	β	Q_α	Q_β
km	km/sec	km/sec	km/sec	km/sec	km/sec	km/sec		
0.250	2.718	2.446	2.650	2.579	2.418	2.268	59.0	29.5
0.250	3.276	2.995	3.183	3.049	2.975	2.790	68.0	34.0
0.250	3.448	3.128	3.345	3.104	3.134	2.877	124.0	62.0
0.250	3.534	3.217	3.421	3.110	3.235	2.944	212.0	106.0
0.250	3.783	3.495	3.661	3.334	3.505	3.202	290.0	145.0
0.250	3.878	3.611	3.751	3.427	3.607	3.301	355.0	177.5
0.250	3.832	3.614	3.751	3.429	3.603	3.306	423.0	211.5
0.250	3.834	3.600	3.753	3.426	3.593	3.322	510.0	255.0
0.500	3.836	3.577	3.758	3.423	3.586	3.356	639.0	319.5
0.500	3.838	3.567	3.766	3.442	3.601	3.433	852.0	426.0
0.500	3.840	3.589	3.777	3.501	3.641	3.539	1278.0	639.0
	3.815	3.667	3.808	3.621	3.721	3.683	2557.0	1278.5

REFERENCES

Herrmann, R. B., and Al-Eqabi, G. I., 1991, Surface wave inversion for shear wave velocity: *in* Hovem, J. M., Richardson, M. D., and Stoll R. D., Eds., Shear waves in marine sediments: Kluwer Academic Publisher, Netherlands, 545-556.

Keilis-Borok, V. I., Levshin, A. L., Yanovskaya, T. B., Lander, A. V., Bukchin, B. G., Barmin, M. P., Ratnikova, L. I., and Its, E. N., 1989,. Seismic surface waves in a laterally inhomogeneous earth: Kluwer Academic Publishers.

Klemperer, S. L., and Luetgert, J. H., 1987, A comparison of reflection and refraction processing and interpretation methods applied to conventional refraction data from Coastal Maine: Bull. Seis. Soc. Am., 77, 614-630.

Luetgert, J., Stewart, D., Unger, J., and Phillips, J., 1989, The extension of Grenville basement beneath the Northern Appalachians: result from the Quebec-Maine seismic reflection and refraction surveys: Tectonics, 8, 677-696.

Mari, J. L., 1984, Estimation of static correction for shear-wave profiling using the dispersion properties of Love waves: Geophysics, 49, 1169-1179.

McMechan, G. A., and Yedlin, M. J., 1981, Analysis of dispersive waves by wave field transformation: Geophysics, 46, 869-874.

Mokhtar, T. A., Herrmann, R. B., and Russell, D. R., 1988, Seismic velocity and Q model for the shallow structure of the Arabian shield from short-

period Rayleigh waves: Geophysics, 53, 1379-1387.
Murphy, J. M., and Luetgert, J. H., 1986, Data report for Maine-Quebec cross-strike seismic-refraction profile: U. S. Geological Survey Open-file Report 86-47, Menlo Park, CA.
Murphy, J. M., and Luetgert J. H., 1987, Data report for the Maine along-strike seismic-refraction profiles: U. S. Geological Survey Open-file Report 87-1331, Menlo Park, CA.
Nolet, G., 1990, Partitioned waveform inversion and two-dimensional structure under the network of autonomously recording seismographs: J. Geophys. Res., 95, 8499-8512.
Osberg, P. H., Hussey II, A. M., and Boonea, G. M., editors, 1985, Bedrock geologic map of Maine: 1:500,000, Maine Geological Survey.
Russell, D. R., 1987, Multi-channel processing of dispersed surface waves: Ph. D. dissertation, Saint Louis University.
Rothman, D. H. 1986, Automatic Estimation of Large Residual Static Correction: Geophysics, 51, 332-346.
Wiggins, R. A., Larner, K. L., and Wisecup, R. D., 1976, Residual static analysis as a general linear inverse problem: Geophysics, 41, 922-938.

GEOPHYSICAL TECHNIQUES FOR CHARACTERIZING SHALLOW VELOCITY-ATTENUATION MODELS

G. I. Al-Eqabi and R. B. Herrmann

Department of Earth and Atmospheric Sciences
Saint Louis University
3507 Laclede Avenue
St. Louis, MO 63103

ABSTRACT

Knowledge of seismic shear wave velocity and Q is required for both seismic hazard analysis and the siting of critical structures since these parameters govern the transmission of the seismic signal from the earthquake to the site and also control the site response itself. These parameters vary spatially and may not be readily available. The purpose of this paper is to show how these can be estimated using surface-wave analysis techniques.

Data from USGS refraction surveys in Maine were selected which show dispersed short-period Rg waves (fundamental mode Rayleigh waves). Processing techniques applied to the data include filtering, waveform inversion of selected trace, phase velocity stacking, interactive amplitude processing, inversion of dispersion parameters for a layered shear-wave velocity and Q model, and finally verifying the derived velocity-attenuation models by comparing both shape, absolute-amplitude and arrival times of synthetic and observed time series. The resultant velocity models show that the shear-wave velocity varies between 2.43-2.81 km/sec for surface layer and Q_β is less than 50 in the upper kilometer of the metamorphic terrain of Maine. The models correlate with the type of geologic rocks encountered. While the study focused on upper crustal structure, the techniques and experimental procedure can be used for shallow site characterization by appropriate scaling of the data acquisition.

INTRODUCTION

The analysis of surface wave dispersion provides a convenient method for determining the elastic properties of a medium. One can use either Rayleigh or Love wave signals. By inverting their phase and group velocity dispersion and frequency dependent anelastic attenuation, a shear-wave velocity and Q model can be obtained. The depth extent and vertical resolution of the earth models is a function of the largest and smallest frequencies observed in the signal. Shallow refraction surveys and quarry blasts are good generators of Rg waves, the short period Rayleigh wave. These waves are characterized by their large amplitudes and clear dispersion. The Rg

waves, because of their high frequencies relative to long period teleseismic observations, are confined to shallow depths, which makes these waves a very good diagnostic tool in studying the shallow structure. Typically they will not sample earth structure as deeply as the observed P- and S-wave arrivals.

THE SEISMIC REFRACTION DATA SET

In the fall of 1984, the USGS collected 850 km of seismic refraction data in Maine (Murphy and Luetgert, 1986; Murphy and Luetgert, 1987). It includes one major profile of more than 300 km, running perpendicular to the strike of the dominant structure and crossing the major tectono-stratigraphic units of east and central Maine, and four shorter profiles extending parallel to the strike and sampling individual tectonic units. Each profile consists of several observation lines. Each line included several shots with the 120 vertical component instruments deployed spatially over 90 km spreads. The receiver and shot locations are believed to be accurate within 15 m. The error in geophone location, relative elevation and timing are considered negligible and less than the error in travel-time due to the changes in weathering zone velocity or thickness (Klemperer and Luetgert, 1987). Two data sets are selected to illustrate the use of surface waves in determining shallow shear-wave velocity and Q structure. These are from profiles SP13-NEG and SP26-NEG, which are parallel to the structural trend in Maine. Figure 1 shows the two shots and their observations points. These two profiles were chosen because of the lack of observable lateral variation in the surface dispersion along the paths. These simple data sets are displayed in Figures 2 and 3. The observed data have been bandpass filtered between 0.5 and 5.0 Hz using a four pole, two zero, Butterworth filter. The data are plotted as a function of reduced travel time and distance. For the SP13-NEG profile, distinct P- and S-wave arrivals can be seen.

REGIONAL GEOLOGIC SETTING

Most of the State of Maine is underlain by tightly folded metasedimentary sequences of Ordovician to Devonian age. The major structural feature in which the SP13-NEG path falls is the Central Merrimack Synclinorium. The synclinorium consists of tightly folded faulted metasedimentary sequences and turbidites of Ordovician to Devonian age. The SP26-NEG path falls within the volcanic belt along the coast of Maine. The surface geology along the profiles varies significantly in lithology and geologic age reflecting the complicated geologic past. The rocks of SP13-NEG path are interbedded pelite and sandstone, whereas those of the SP26-NEG are mostly volcanics (Osberg and others, 1985).

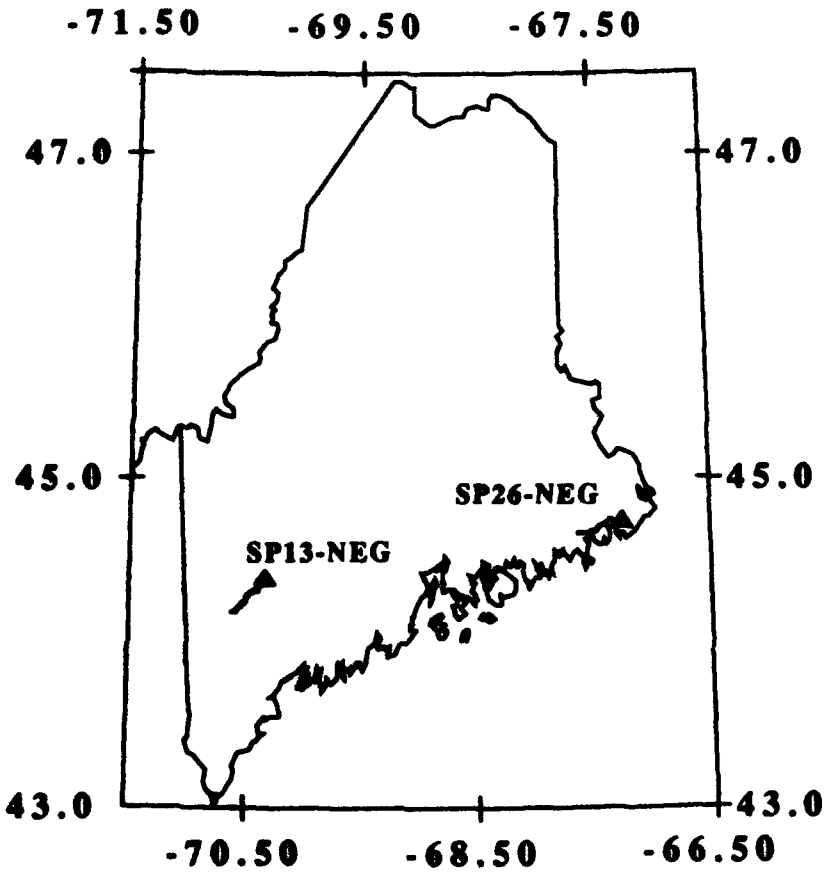

Fig. 1. Map showing the State of Maine and the locations of the two shot points (triangles) and the observation points for each shot point. Shot point SP13-NEG is in the southwest part of the state, while SP26-NEG is in the eastern part of the State.

DATA PROCESSING AND ANALYSIS

The recorded multichannel refraction data sets show excellent Rg-wave dispersion. Processing techniques were developed that could be applied efficiently to obtain the desired shear-wave velocity and Q structure. The techniques are based on either performing direct inversion of waveforms for the shear-wave velocity model or extracting the dispersion and anelastic attenuation coefficients that are then inverted for the shear-velocity and Q models. The data sets are first p–ω stacked to obtain phase velocity curves. The anelastic coefficient data are obtained after extracting spectral amplitudes by applying multiple-filter analysis followed by interactively processing the amplitudes to determine their spatial anelastic attenuation. The phase velocity and anelastic dispersion data are then inverted to obtain the shear-wave velocity and Q models. While the multiple filter analysis also yields useful group velocity information, this is not used because of the excellent phase velocity data and also because of the desire to demonstrate that the earth

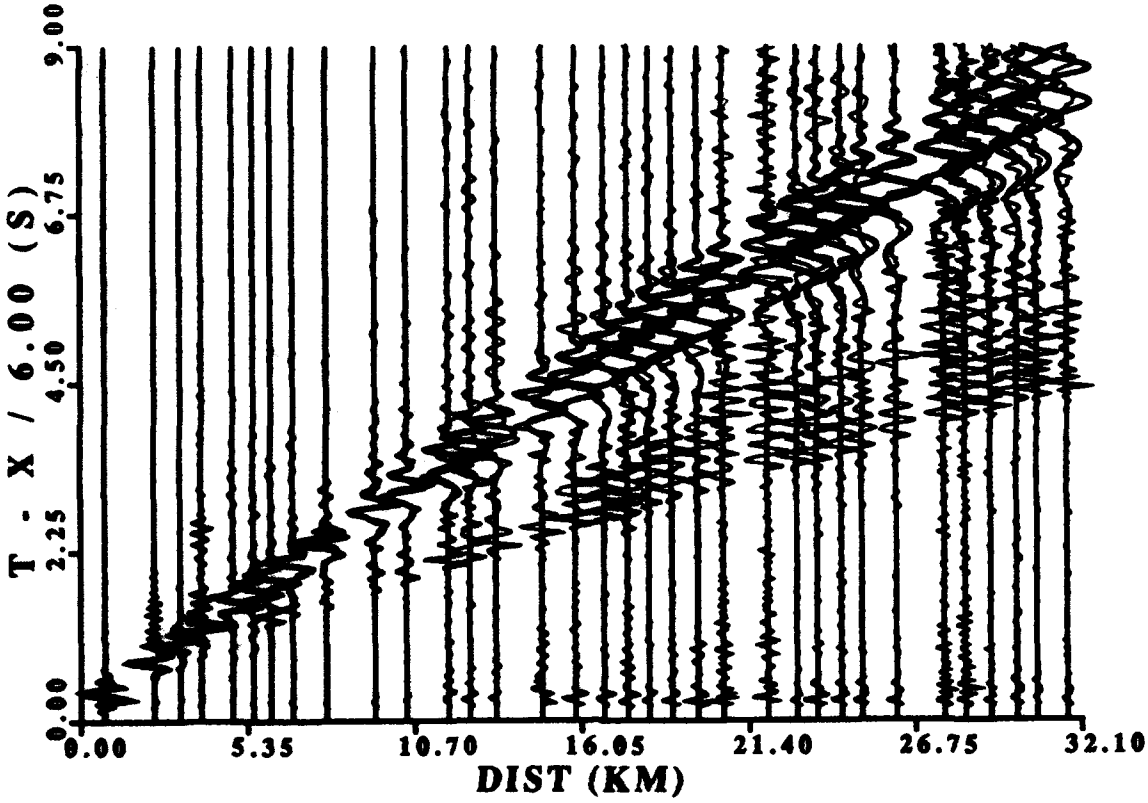

Fig. 2. Data set used for the SP13-NEG profile. The light traces are the observed data. The heavy traces are the forward synthetic data derived from the inverted velocity and Q models.

model can predict the observed time histories.

$p-\omega$ Stacking

The $p-\omega$ stacking technique is used to obtain phase velocity dispersion without making assumptions about source phase or the number of wavelengths between the source and single receiver, both of which add ambiguity to one- or two-station phase velocity estimation techniques. This technique provides excellent results when processing multichannel data by being able to isolate individual normal modes of propagation. It involves two transformations, a $p-\tau$ stack followed by a Fourier transform over τ. (McMechan and Yedlin, 1981; Russell, 1987; Mokhtar and others, 1988; Herrmann and Aleqabi, 1991).

The seismic waves observed at a distance, x_n, can be represented as a sum of superimposed modes as

$$f_n(x,t) = \frac{1}{2\pi}\int_{-\infty}^{\infty}\sum_m A_m(x,\omega)e^{i\omega t}\,d\omega \qquad (1)$$

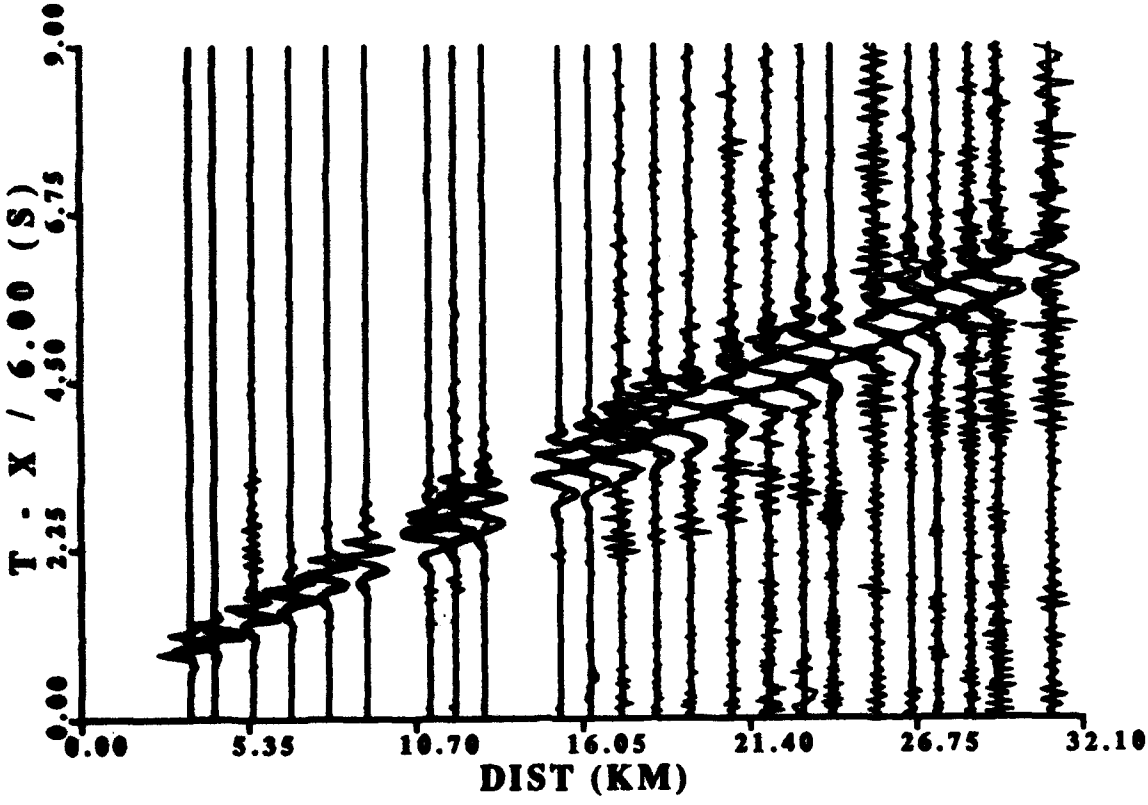

Fig. 3. Data set used for the SP26-NEG profile. The light traces are the observed data. The heavy traces are the forward synthetic data derived from the inverted velocity and Q models.

where

$$A_m(x,\omega) = I(\omega)\, S_m(\omega) R_m(\omega)\, \frac{e^{-\gamma_m(\omega)\, x_n}}{\sqrt{x_n}}\, e^{-i\, k_m(\omega) x_n}\,, \tag{2}$$

m is the mode number, $I(\omega)$ the instrument response (complex), $S_m(\omega)$ the source spectrum (complex), $R_m(\omega)$ the path response (real), and $\gamma_m(\omega)$ the attenuation coefficient (real). The wavenumber k is related to the phase velocity c by the relation $k = \omega/c$. If the Fourier transform of (1) is defined as $F_n(x,\omega)$, the $p-\omega$ stack is defined here as

$$F(p,\omega) = \sum_n \sqrt{x_n} F_n(x,\omega) e^{i\omega p x_n} \tag{3}$$

or explicitly as

$$F(p,\omega) = \sum_n \sum_m \sqrt{x_n}\, A_m(\omega, x_n) e^{i(\omega p - k_m(\omega))x_n}. \tag{4}$$

If the signal consists of a single mode, then it is easy to see that this summation becomes extremal if $\omega p = k_n$. By evaluating $| F(p,\omega) |$ as a function of

p for a fixed frequency, one can search for the values of p that make the expression extremal. p is related to the phase velocity, c, by the simple relation $p = 1/c$. For multimode signals, secondary extrema will occur, which may give the dispersion of another mode. Since modal excitation is frequency dependent, different modes will dominate at different frequencies.

Multiple Filter Analysis

Multiple filter analysis was introduced by Dziewonski and others (1969) for the purpose of extracting the surface-wave group velocities and spectral amplitudes from dispersed waveform. Define the Fourier transform of a dispersed propagating seismic signal at distance x by $A(x,\omega)e^{-i(k(\omega)x-\phi)}$ and, a Gaussian filter as

$$H(\omega) = \begin{cases} e^{-\alpha(\omega-\omega_0)^2/\omega_0^2} & |\omega-\omega_0| \le \omega_c \\ 0 & |\omega-\omega_0| > \omega_c \end{cases} \tag{5}$$

where $\omega_c = \omega_0(\pi/\alpha)^{1/4}$, α is a filter parameter controlling the tradeoff between time domain and frequency domain resolution, ω_0 is the filter center frequency and ω_c is the filter cutoff frequency. The result of applying this filter to the dispersed signal is a time domain signal whose envelope reaches a maximum at the group velocity arrival times and given is by Herrmann (1973) as

$$g(t,x) = \frac{A(\omega_0,x)\omega_0}{2\pi}\left(\frac{\pi}{\alpha}\right)^{1/4} e^{-\omega_0^2(t-x/U_0)^2/4\alpha} \tag{6}$$

where U_0 is the group velocity.

Computationally, the time series is filtered using (5), a Hilbert transform of the filtered time series is taken, and the two are combined to form the envelope. The envelope is searched for the relative maxima, g_{max}, from which the group velocity is computed. The spectral amplitude is estimated from (6) by the relation

$$A(x,\omega_0) = g_{max}(2\pi/\omega_0)(\alpha/\pi)^{1/4}$$

A given set of seismic traces can be processed using multiple filter analysis individually or as a group. Assuming a laterally homogeneous waveguide, the result of a single trace processing could be utilized to obtain adequate earth structure. For a group of traces we could use two approaches for estimating the average velocity and anelastic attenuation. We can run multiple filter analysis for each trace and consolidate the individual group velocity and spectral amplitude estimates into a large file and use an interactive computer program to manually isolate modes on the basis of a group velocity window, and then use all information associated with that window to determine a mean group velocity and an anelastic attenuation coefficient, γ, from the decay of amplitude with distance. The model use to obtain γ is that the spectral amplitudes of a single mode and frequency vary with distance according to the relation

$$A(x,\omega) = A_0 e^{-\gamma x}/\sqrt{x}$$

The second way of analyzing group of traces for average group velocity and average anelastic attenuation coefficients is to implement the group velocity stack concept of Barker (1988). The idea is to obtain narrow band pass Gaussian filter of each trace, in a manner of (5), and then to stack the envelopes of different traces for a given frequency after transforming the envelopes from function of time to function of group velocity. A search then is performed to find the stack maximum amplitude which defines the group velocity. Using this information, the spectral amplitudes associated with the corresponding group arrival time can be extracted from the original filtered traces, and a regression performed to obtain γ. Spectral amplitudes can be used to estimate the anelastic attenuation coefficient.

Surface-Wave Dispersion Inversion

An implicit theoretical relationship exists between modes, phase and group velocities, and the structural earth parameters such as shear velocity and density. By combining linear inversion theory with variational techniques to evaluate necessary partial derivatives with respect to model parameters, the data can be inverted to obtain an earth model (Russell, 1987). A linear iterative inversion scheme can be used to minimize the difference between observed and predicted phase velocity,

$$c_{obs} - c_{pred} = \frac{\partial c}{\partial \beta_1}\Delta\beta_1 + \ldots + \frac{\partial c}{\partial \beta_n}\Delta\beta_n + \frac{\partial c}{\partial Q_{\beta_1}^{-1}}\Delta Q_{\beta_1}^{-1} + \ldots + \frac{\partial c}{\partial Q_{\beta_n}}\Delta Q_{\beta_n}^{-1}, \quad (7)$$

group velocity,

$$U_{obs} - U_{pred} = \frac{\partial U}{\partial \beta_1}\Delta\beta_1 + \ldots + \frac{\partial U}{\partial \beta_n}\Delta\beta_n + \frac{\partial U}{\partial Q_{\beta_1}^{-1}}\Delta Q_{\beta_1}^{-1} + \ldots + \frac{\partial U}{\partial Q_{\beta_n}}\Delta Q_{\beta_n}^{-1} \quad (8)$$

and anelastic attenuation coefficients,

$$\gamma_{obs} - \gamma_{pred} = \frac{\partial \gamma}{\partial \beta_1}\Delta\beta_1 + \ldots + \frac{\partial \gamma}{\partial \beta_n}\Delta\beta_n + \frac{\partial \gamma}{\partial Q_{\beta_1}^{-1}}\Delta Q_{\beta_1}^{-1} + \ldots + \frac{\partial \gamma}{\partial Q_{\beta_n}}\Delta Q_{\beta_n}^{-1} \quad (9)$$

The resulting system of linear equations can be solved using inversion theory to find shear-wave velocity and Q structure. The system of the entire set of observed data will have the matrix form

$$\mathbf{Y} = \mathbf{A}\mathbf{X} + \epsilon \quad (10)$$

where, Y is an $m \times 1$ is the vector of differences between theoretical dispersion data and observed dispersion data. X is an $n \times 1$ is vector of unknown parameters, ϵ is an $m \times 1$ is a vector of residuals, and the kernel matrix A is an $m \times n$ matrix consisting of the partial derivatives of dispersion parameters with respect to starting model parameters. By the least squares principle, a set of model parameters, X, is considered a valid solution if it will minimize the sum of the squares of the residuals, ϵ.

To simplify the minimization process, Lawson and Hanson (1974) introduced a singular value decomposition, which is an orthogonal transformation

of the matrix **A** into three matrices and can be written as $\mathbf{A} = \mathbf{U}\Lambda\mathbf{V}^T$ where, **U** is an $m \times m$ orthogonal matrix, **V** an $n \times n$ orthogonal matrix, and Λ an $m \times n$ diagonal matrix. Since an "orthogonal matrix" is a matrix whose transpose is also its inverse. the solution vector **X** is given by $\mathbf{X} = \mathbf{V}\Lambda^{-1}\mathbf{U}^T\mathbf{Y}$ or equivalently $\mathbf{X} = (\mathbf{A}^T\mathbf{A})^{-1}\mathbf{A}^T\mathbf{Y}$.

In situations where the inversion problem is poorly constrained, at least one of the singular values λ_j will be small or zero, causing an excessive magnification of the corresponding vector $\mathbf{v}_j$. This instability in the solution can be controlled by adding the constraint of keeping the size of $\sigma^2\mathbf{X}^T\mathbf{X}$ small. The corresponding solution vector is

$$\mathbf{X} = (\mathbf{A}^T\mathbf{A} + \sigma^2\mathbf{I})^{-1}\mathbf{A}^T\mathbf{Y} \tag{11}$$

where σ is the damping value and **I** is the identity matrix. If the damping parameter σ is increased, more weight is imposed on minimizing the solution norm, and less on reducing the least-squares residuals, and if it set $\sigma^2 = 0$ the problem of the stochastic least-squares will be reduced to standard least-squares problem. In our formulation the solution vector **X** represents changes in the shear velocities and inverse Q, and is used to update the starting model. The process starts again with this new model and is repeated until the desired level of convergence is obtained.

Waveform Inversion

The waveform inversion procedure uses waveform data to find the model parameter, ξ, which minimizes the difference between the observed time histories, $s(x_j,t)$ and the theoretical seismograms $u(x_j,t,\xi)$. ξ represents model parameters and could include velocity, density, Q structure, source location and mechanism. Generally, *a priori* knowledge and some parameter assumptions are required. Mathematically, the minimization problem can be written as

$$F(\xi) = \frac{1}{q}\int_0^T | u(t,x,\xi) - S(t,x) |^q dt \tag{12}$$

where q = the norm, T = time span, and $F(\xi)$ = the objective function. The solution to the above optimization problem is to find the vector ξ (i.e., the model) that minimizes the function $F(\xi)$. A detailed discussion of this scheme is presented by Nolet and others (1986) and Nolet (1987, 1990).

Synthetic Seismograms

In a homogeneous earth model, the Fourier spectrum for single mode recorded at receiver distance r and depth z from the a source at depth h is

$$u(r,\phi,z,\omega) = e^{\frac{-i\pi}{4}} \frac{e^{-ikr}}{\sqrt{2\pi kr}} \frac{\epsilon V(\omega,z)}{(2cUI_0)^{1/2}} \frac{W(\omega,h)}{(2cUI_0)^{1/2}} \tag{13}$$

where ω is the angular frequency, k is the wave number, c is the phase velocity, U is the group velocity, and I_0 is the energy integral. ϵ is either a real or imaginary number, depending upon the component of motion. $V(\omega,z)$ is the eigenfunction sampled at the receiver, and $W(\omega,z)$ is a source mechanism

dependent linear combination of eigenfunctions at the source. The term $A = 1/(2CUI_0)$ is called the amplitude response. The four terms in the equation represent, respectively the phase term from the Hankel function, the propagation phase term from Hankel function, the sampling of the wavefield at the receiver, and the sampling of the excitation at the source.

SEISMIC VELOCITY MODELS

Figure 4 shows the multichannel phase velocity stack for SP13-NEG path. The inversion started with a twelve layered earth model with velocities and densities of each layer equal to that of the halfspace. Table 1 presents the resulting shear-wave velocity values for this path. The velocities in the lower part of the model are not well resolved. Also shown in the same table are the Q_β values for this path. These values were obtained by inverting the anelastic attenuation coefficients, γ, obtained from the interactive processing of the spectral amplitudes. Table 2 gives the shear-wave velocity model for the SP26-NEG path obtained from applying the waveform inversion technique to the single trace at a distance of 15.13 from the source. The Q_β model for path SP26-NEG (Table 2) was obtained by inverting observed anelastic coefficient obtained from multichannel group velocity and anelastic coefficient stacking techniques (Barker, 1988). The shear-wave velocities of the SP26-NEG path are higher than those of the SP13-NEG path and this is expected since the SP26-NEG path lies within the metavolcanic rocks of the coastal lithotectonic unit, whereas the SP13-NEG path lies within the Central Merrimack Synclinorium with mostly interbedded pelite and sandstone rocks.

SYNTHETIC SEISMOGRAMS

For the laterally homogeneous models derived in this study (Tables 1 and 2), synthetic Rg wave seismograms were calculated assuming a step source time function. The synthetic seismograms were passed through a second order Butterworth filter with a low-cut corner frequency at 2 Hz to approximate the sensor response of the original data, and then both observed and synthetic seismograms were band-pass filtered between 0.5-5.0 Hz to emphasize the Rg wave. Figures 2 and 3 compare the synthetic fundamental mode seismograms and the original data for paths SP13-NEG and SP26-NEG, respectively. An excellent fit is obtained in both surface-wave shape and arrival time at a given distance. Other displays have shown an excellent fit to peak amplitudes as a function of distance, thus supporting the Q_β model found.

DISCUSSION AND CONCLUSIONS

This study focused on presenting geophysical techniques for the evaluation of the shallow shear velocity structures, utilizing high frequency Rayleigh waves (Rg) recorded by the USGS during the Maine refraction experiment. A variety of geophysical processing techniques were applied to the data sets among them, filtering, phase velocity stacking, waveform inversion of selected traces, inversion of phase velocity and synthetic seismogram calculation.

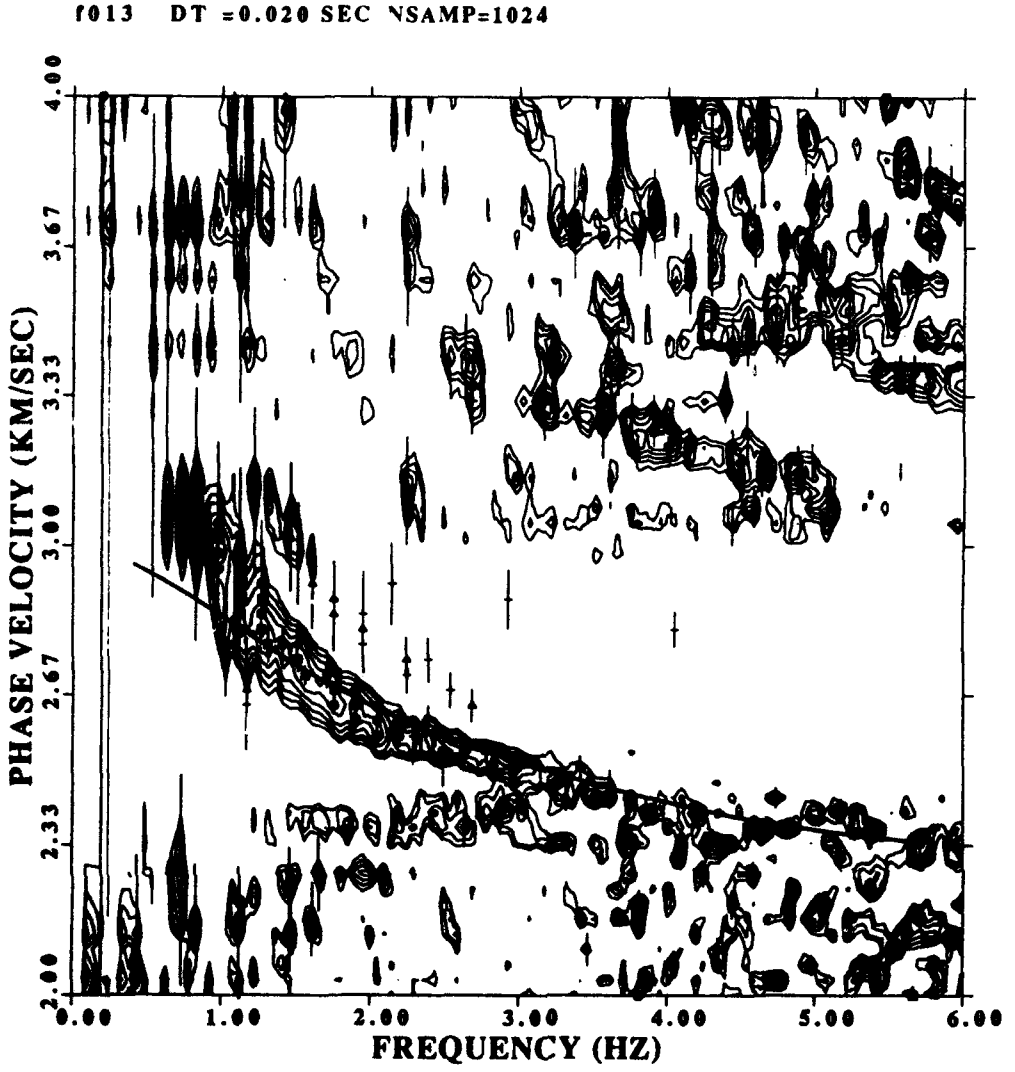

Fig. 4. Result of the p–ω stack for the traces in Figure 2. The stack values are contoured as a function of phase velocity and frequency. Large amplitudes are seen along the locus of the actual dispersion curve, for what may be higher modes, and for stack noise due to spatial and temporal aliasing. The fundamental mode phase velocity dispersion curve from the inverted model is also shown.

The stacking techniques require some manual intervention to correctly define the dispersion data for a given mode. This is required since different modes are dominant at different frequencies. This complicates the dispersion data selection. Other complicating factors arise from the medium geometry, lateral velocity variations and spatial attenuation. When no lateral variation in the earth model is expected, then a single well dispersed trace is sufficient to define the earth model, as was done with the data of Figure 3. To estimate the anelastic attenuation of this data set, the group velocity stacking concept of Barker (1988) was used to automatically estimate the anelastic attenuation

Table 1
Velocity and Q_β Model for SP13NEG

Layer Thickness km	Compressional velocity km/sec	Shear velocity km/sec	Density gm/cc	Q_α	Q_β
0.250	4.218	2.435	2.350	63.0	31.50
0.250	4.990	2.881	2.498	65.0	32.55
0.250	5.094	2.941	2.519	73.0	36.50
0.250	5.493	3.233	2.598	82.0	41.00
0.250	5.636	3.254	2.627	92.0	46.00
0.250	5.725	3.305	2.645	106.0	53.00
0.250	5.756	3.323	2.651	124.0	62.00
0.250	5.767	3.330	2.653	148.0	74.00
0.500	5.770	3.331	2.654	185.0	92.50
0.500	5.770	3.331	2.654	247.0	123.50
0.500	5.770	3.331	2.654	371.0	185.50
	5.770	3.331	2.654	743.0	371.50

coefficients, γ. The success in matching the observed time histories indicates that it may be possible to automatically process such data without too much analyst intervention.

In spite of limitations of the processing techniques used, frequency content of the data, and the geologic complexity of the area, the analysis provided important information that can characterize the subsurface along the processed paths in Maine. Higher velocities are observed (2.816 km/sec in top layer) for paths where metavolcanic rocks are observed (SP26-NEG). Lower velocities were observed (2.435 km/sec in the top layer) on the SP13-NEG path, where the rocks are mostly interbedded sandstone and pelite. The values of Q_β are less than 50 in the top 1 km for both paths. Such low values also have also been found by Mokhtar and Herrmann (1988) for the Arabian shield. The exact cause for such low Q_β values cannot be explicitly attributed to changes in lithology but may be related more to the formation pore geometry, fluid content, and crack density all acting together.

The techniques presented here can be applied to problems of other scales. For example if the refraction experiment is performed over a 3 km spread, and frequencies of 10 - 30 Hz are used, one should be able to invert for the shear wave velocity and Q in the upper 300m. Shorter spreads would focus on proportionately shallower depths. The use of surface waves does not require drilling and logging, is essentially non-invasive and results can be obtained fairly rapidly, with all the processing performed on an ordinary PC. The shear-wave velocity is directly related to the shear modulus of the

Table 2
Velocity and Q_β Model for SP26-NEG

Layer Thickness km	Compressional velocity km/sec	Shear velocity km/sec	Density gm/cc	Q_α	Q_β
0.250	4.877	2.816	2.507	56.0	28.00
0.250	5.845	3.372	2.681	59.0	29.50
0.250	5.912	3.410	2.681	65.0	32.50
0.250	5.997	3.460	2.735	77.0	38.50
0.250	6.163	3.555	2.785	90.0	45.00
0.250	6.387	3.684	2.852	105.0	52.50
0.250	6.491	3.745	2.859	123.0	61.50
0.250	6.696	3.863	2.905	147.0	73.50
0.500	6.845	3.949	2.939	184.0	92.00
0.500	6.859	3.957	2.943	246.0	123.00
0.500	6.867	3.962	2.945	369.0	184.50
	6.885	3.972	2.950	738.0	369.00

material and is thus an important parameter for engineering design.

ACKNOWLEDGMENTS

The assistance of W. Kohler and W. Mooney of the USGS in providing the data set is appreciated. We thank Prof. G. Nolet of the University of the Netherlands for fruitful discussions and for supplying a version of his waveform inversion s software.

REFERENCES

Barker, T., 1988, Array processing of Rayleigh waves for shallow shear wave velocity structure (abs): Seismological Research letters, v. 59, p. 12.

Dziewonski, A. M., Bloch, S. and Landisman, M., 1969, A technique for the analysis of transient seismic signals: Bulletin of the Seismological Society of America, v. 59, p.427-444.

Herrmann, R. B., 1973, Some aspects of band-pass filtering of surface wave: Bulletin of the Seismological Society of America, v. 63, p. 663-671.

Herrmann, R. B., and Aleqabi, G. I., 1991, Surface wave inversion for shear wave velocity: *in* Hovem, J. M., Richardson, M. D., and Stoll, R. D., eds., Shear waves in marine sediments: Netherlands, Kluwer Academic Publisher, p. 545-556.

Klemperer, S. L., and Luetgert, J. H., 1987, A comparison of reflection and refraction processing and interpretation methods applied to conventional refraction data from Coastal Maine: Bulletin of the Seismological Society of America, v. 77, p. 614-630.

Lawson, C. L., and Hanson, R. J., 1974, Solving least-squares problems: New Jersey, Prentice-Hall, 340p.

McMechan, G. A., and Yedlin, M. J., 1981, Analysis of dispersive waves by wave field transformation: Geophysics, v. 46, p. 869-874.

Mokhtar, T. A., Herrmann, R. B., and Russell, D. R., 1988, Seismic velocity and Q model for the shallow structure of the Arabian shield from short-period Rayleigh waves: Geophysics, v. 53, p. 1379-1387.

Murphy, J. M., and Luetgert, J. H., 1986, Data report for Maine-Quebec cross-strike seismic-refraction profile: California, U. S. Geological Survey Open-file Report 86-47, 71p.

Murphy, J. M., and Luetgert. J. H., 1987, Data report for the Maine along-strike seismic-refraction profiles: California, U. S. Geological Survey Open-file Report 87-133, 134p.

Nolet, G., 1987, Waveform tomography: *in* Nolet, G., eds., Seismic Tomography, Massachusetts , D. Reidel, pp. 301-322

Nolet, G., 1990, Partitioned waveform inversion and two-dimensional structure under the network of autonomously recording seismograph: Journal of Geophysical Research, v. 95, p. 8499-8512.

Nolet, G., Trier, J. V., and Huisman, R. 1986, A formalism for nonlinear inversion of seismic surface waves: Geophysical Research Letters, v. 13, p. 26-29.

Osberg, P. H., Hussey II, A. M., and Boonea, G. M., eds., 1985, Bedrock geologic map of Maine, 1:500,000: Maine Geological Survey.

Russell, D. R., 1987, Multi-channel processing of dispersed surface waves: [Ph.D. dissertation]: St. Louis, Missouri, St. Louis University, 150p.

ISOTROPIC MOMENT - YIELD RELATIONS FOR SMALL CHEMICAL EXPLOSIONS

R. B. Herrmann, G. Al-Eqabi and K. D. Hutchenson

Department of Earth and Atmospheric Sciences
Saint Louis University
3507 Laclede Avenue
St. Louis, MO 63103

ABSTRACT

Surface wave data from eight chemical explosions along a USGS refraction profile in the State of Maine are used to estimate isotropic moment - yield relations. The moment estimates are obtained by using the surface-wave dispersion data to define an earth model, the decrease of surface-wave amplitudes with distance to define and anelastic attenuation model, and synthetic seismograms for the derived laterally varying model to estimate the source excitation. The frequency dependence of source excitation is considered by comparing observed and predicted time histories after being passed through narrow bandpass filters. A step pressure source time function is adequate for explaining the observed 1-5 Hz short period surface waves. The derived moments are compared to other estimates available in open literature.

INTRODUCTION

The primary focus has been on developing techniques for the estimation of isotropic moment, M_I, from fundamental mode surface-wave data with application to small explosions. Since the frequencies of interest are in the 0.5 - 5.0 Hz, range, path specific structure and anelastic attenuation must be defined before M_I can be estimated. To do this a robust technique for inferring the path effects from a single station recording of an explosion must be developed and then the methodology must be carefully tested before being routinely applied.

We have made extensive use of a USGS-GSC refraction survey in the state of Maine (Murphy and Luetgert, 1986; Murphy and Luetgert, 1987). Figure 1 presents the profiles analyzed. The profiles are interesting since they are either parallel or perpendicular to the structural trend of the Appalachian Mountains in the state.

We noted significant lateral changes in the moveout of the surface-wave train. Figure 2 shows some data acquired from Shot Point 6, in a direction toward Shot Point 7. The observed data have been bandpass filtered between 0.5 and 5.0 Hz. Lateral variation is seen in the observed surface-wave train, center, and also in the S-arrivals, bottom. While some of the S-wave arrival lateral variation could be attributed to an increase of velocity with depth, it occurs at the same places where the surface-wave moveout changes. The arrivals beyond 30 km are delayed, and cannot be explained by refracted arrivals. Other shot also show a strong correlation between the lateral variation in the surface-wave and S-wave arrivals.

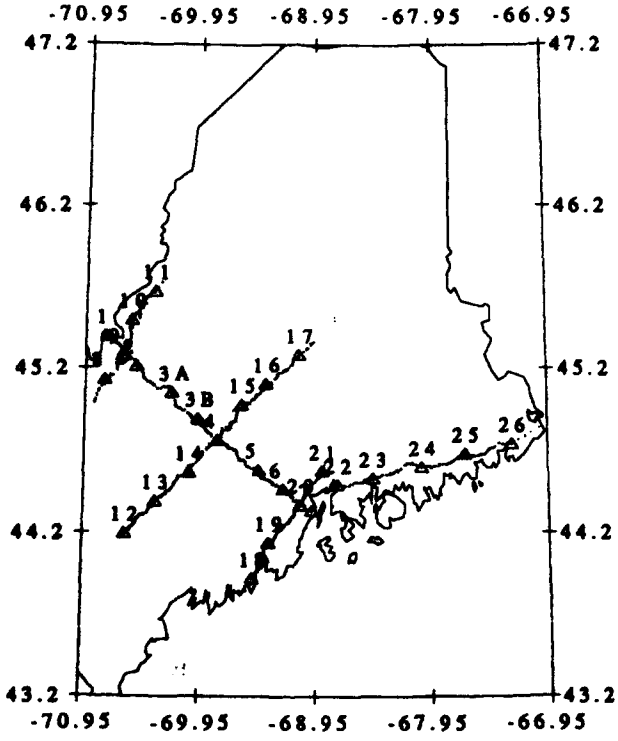

Fig. 1. Location of shotpoints and observation points for the Maine refraction profiles.

By using a sequence of stacking techniques, visual examination, waveform modeling and cross-correlation techniques, a blocklike velocity model was derived (Keilis-Borok *et al*, 1989;Nolet, 1990). Table 1 shows the model developed for this profile. This table shows the width of each block, and the shear-wave velocity values within each block. The same Q model is assumed for each separate velocity block. This model is shown graphically in Figure 3.

ISOTROPIC MOMENT ESTIMATES

One test of the model is to compare both the shape and amplitudes of synthetic time histories. The synthetic time histories are show at the top of Figure 2. The arrival times and waveform shapes are well modeled. Another test is to compare peak amplitudes of the synthetics and observed data in the time domain. This is shown in Figure 4 where the peak amplitudes resulting from different choices of bandpass filters are plotted. In this figure, the individual filter responses are shifted vertically for clarity. The synthetic data are given by solid curves and the observed data are given by the different symbols. This figure shows that the Q model of Table 1 can explain the spatial decay of amplitudes. One final check is the test of the assumption of a step source time function used in the synthetics, by computing M_i for each bandpass filter. If the assumption of the source time function shape is correct, then the isotropic moment estimates from the different bandpass

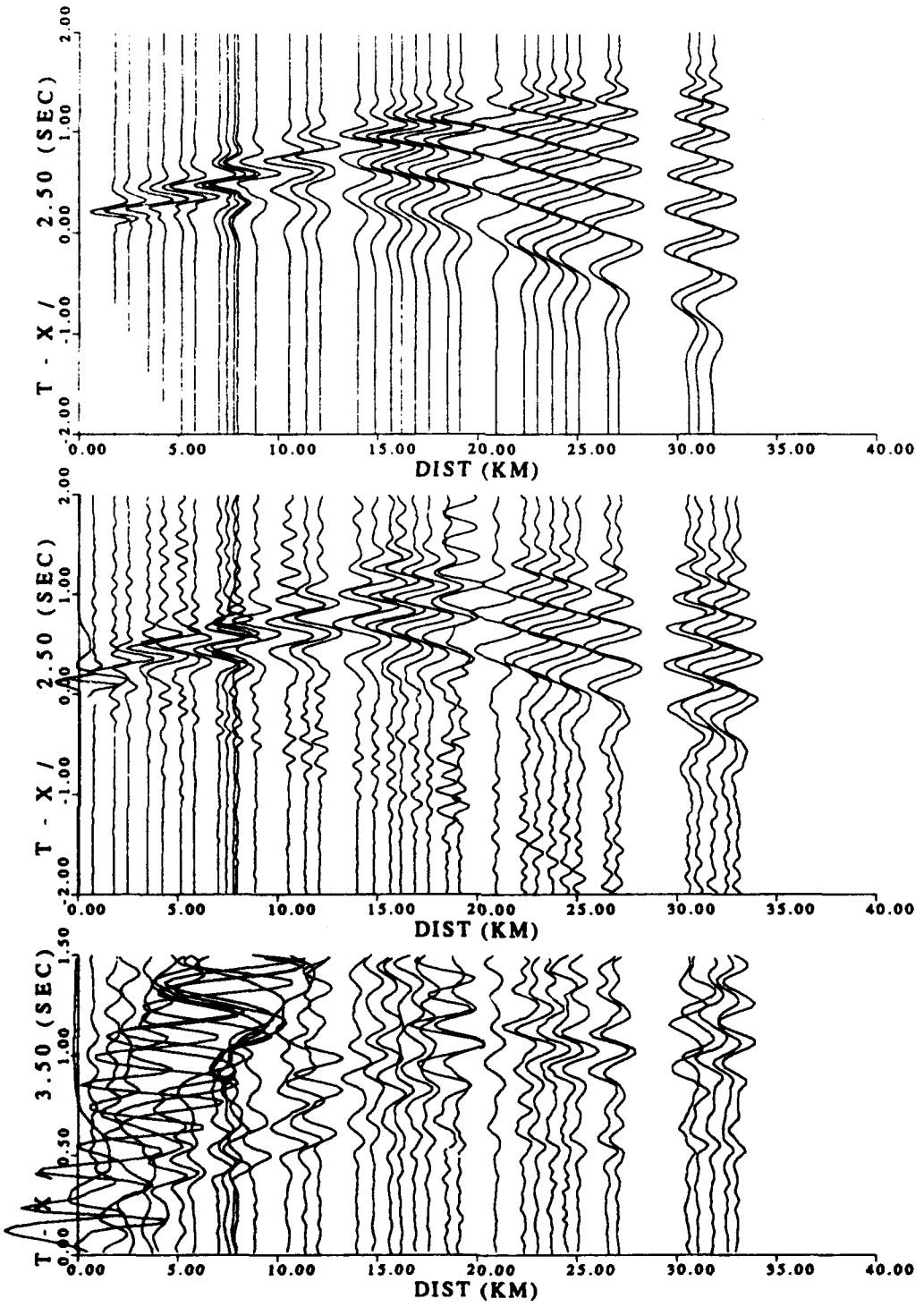

Fig. 2. Seismograms from Shot Point 6. Top) synthetic surface-wave seismograms; Center) observed seismograms displayed with a reduction velocity of 2.5 km/s; Bottom) observed shear wave arrivals displayed with a reduction velocity of 3.5 km/s.

Table 1.
Four Velocity Models and Q_β Structure for
Region A, SP6 Positive Side (SE) Obtained from Waveform
Inversion, Two Station Phase Adjustment Followed by Dispersion Inversion.

Position(km)	Model-1 517 0.0-10.0	Model-2 517-519 10.0-12.0	Model-3 520-526 12.0-19.5	Model-4 526-533 19.5-29.0	Average model	Standard deviation	Q_α	Q_β
H km	β km/sec	β km/sec	β km/sec	β km/sec	β km/sec	σ_β km/sec		
0.250	2.4939	2.3808	2.6091	2.7411	2.5562	0.133810	84.0	42.0
0.250	3.0149	2.8335	3.0871	3.3590	3.0736	0.188894	163.0	81.0
0.250	3.1111	2.9546	3.2009	3.4813	3.1868	0.191414	320.0	160.0
0.250	3.1281	2.9881	3.1980	3.5310	3.2113	0.199446	378.0	189.0
0.250	3.1486	3.0154	3.2264	3.5772	3.2419	0.207765	381.0	190.5
0.250	3.1864	3.0367	3.2655	3.6006	3.2728	0.206011	394.0	197.0
0.250	3.2274	3.0533	3.3012	3.6006	3.2956	0.197741	426.0	213.0
0.250	3.2782	3.0587	3.3242	3.6006	3.3154	0.192804	485.0	242.5
0.500	3.3148	3.0566	3.3336	3.6006	3.3264	0.192460	582.0	291.0
0.500	3.3225	3.0498	3.3336	3.6006	3.3256	0.196202	762.0	381.0
0.500	3.3224	3.0315	3.3336	3.6006	3.3220	0.201333	1134.0	567.0
	3.4699	3.0161	3.3336	3.6006	3.3550	0.217274	2255.0	1127.0

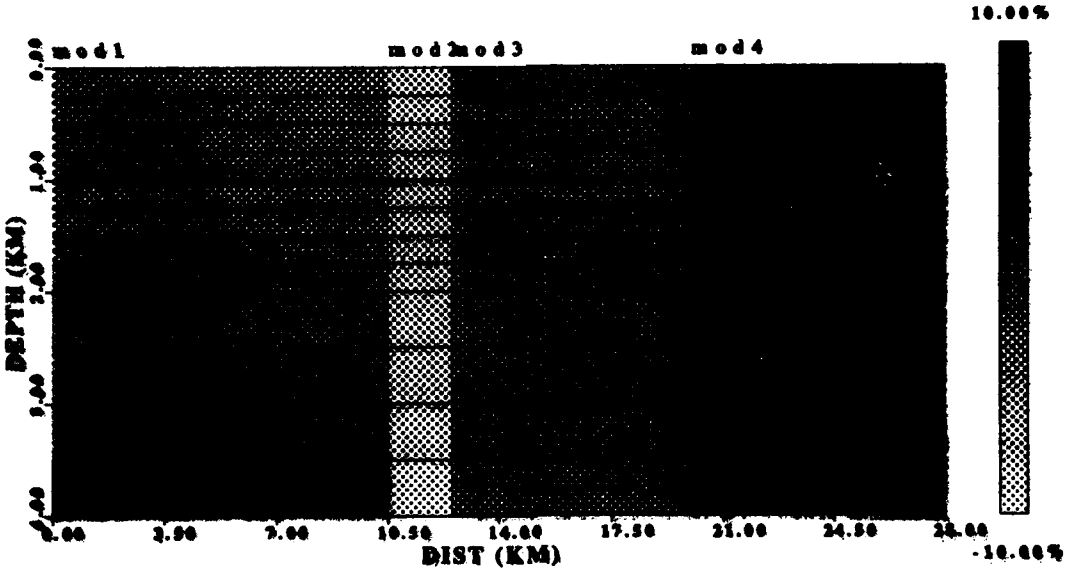

Fig. 3. Presentation of the derived lateraly varying model. For each layer, the shading represents the percent deviation of the layer velocity from an unweighted mean of the lateraly varying velocity.

filtered data sets should agree. Table 2 shows this comparison. The assumption of a step source time function is valid in the frequency range of 0.5-5.0 Hz for this data set. Higher or lower frequency information was not resolved in the data.

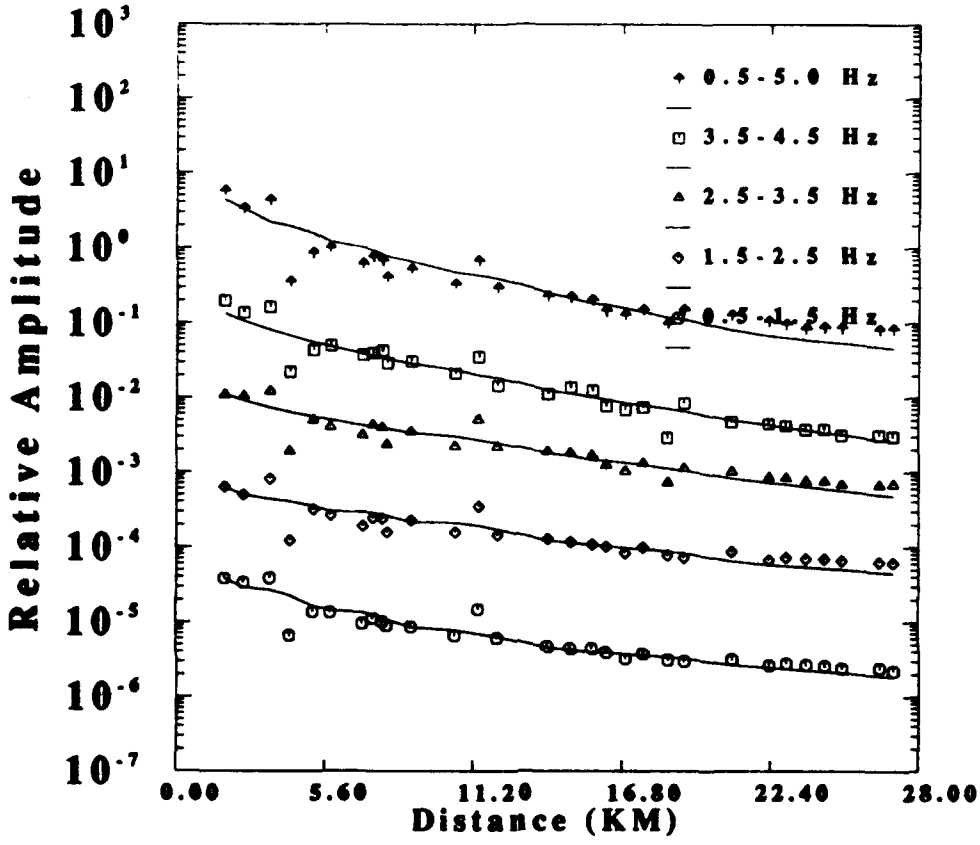

Fig. 4. Comparison of amplitudes of observed (symbols) and synthetic time histories (curves) after being filtered through different bandpass filter bands. The frequencies shown are corners of a Butterworth bandpass filter, which has 12db/octave roll off outside the passband.

We were able to perform this analysis on the data from eight shot points, estimating M_l and also Ψ_∞ for each shot. The Ψ_∞ was estimated using the density and compressional wave velocity at the source depth inferred from the surface-wave inversion. The results of this analysis are compared to other in published literature in Table 3. The comparison is also shown in Figures 5 and 6. Several features stand out. First, the present data set of chemical explosions includes only small yield events. Second, a trend for chemical explosions is not obvious due to the differences in the experiments, e.g., spall, whether shot point physical parameters were known, etc. The possible relationship between the chemical and nuclear explosion populations is not

Table 2. Estimation of M_l from filtered seismograms

Frequency band (Hz)	Isotropic Moment (dyne-cm)	Confidence Factor 1 σ
0.5-1.5	1.99E+18	1.06
1.5-2.5	2.11E+18	1.07
2.5-3.5	2.14E+18	1.06
3.5-4.5	1.77E+18	1.07
0.5-5.0	1.97E+18	1.09

apparent given the lack of overlap.

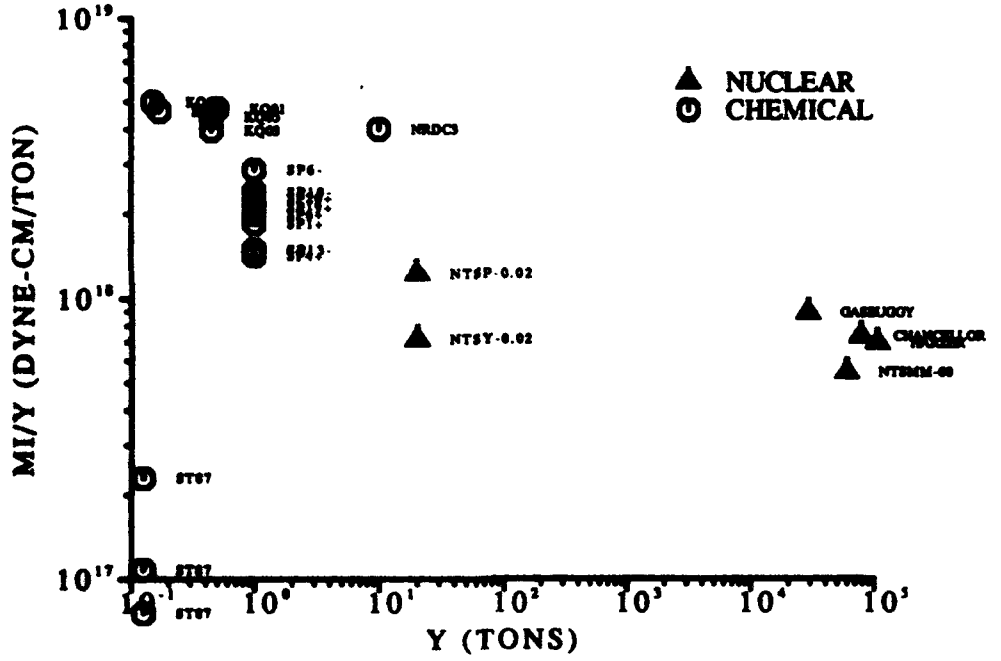

Fig. 5. Comparison of the moment-to-yield ratio as a function of yield for explosions.

CONCLUSIONS AND RECOMMENDATIONS

From the standpoint of wave propagation, the lateral variations observed are large, some as large as 10%. Analysis and modeling of these data require new techniques.

Isotropic moment estimates show variability for nominally the same shot size. Further refinement is not possible since detailed information on shot

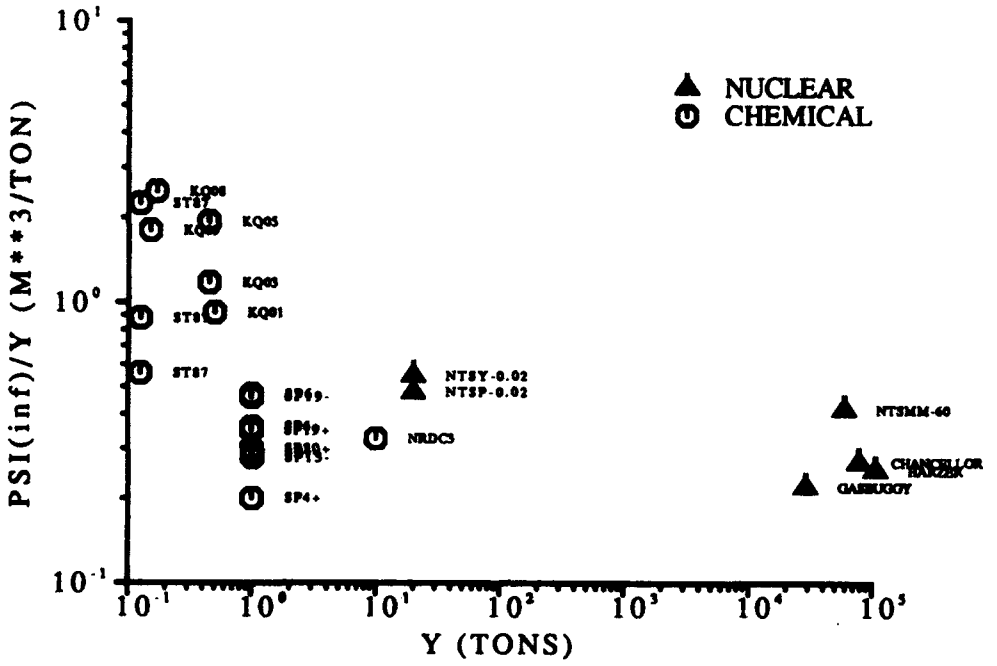

Fig. 6. Comparison of the $\Psi(\infty)$-to-yield ratio as a function of yield for explosion.

emplacement and shot medium properties are not available to us. On the other hand these results good since the multichannel processing gave reliable estimates of dispersion and anelastic attenuation.

To further understand the relation between chemical and nuclear explosion yield estimates, it is necessary to obtain data in the 10 - 100 ton range. A coordinated field experiment to acquire such data from the shot point out to 300 km should be sponsored.

Finally, the data sets considered indicate that a step source time function is appropriate for the moment tensor. For large chemical explosions that are part of an industrial process, the distributed nature of the source together with the time delays used in blasting would be expected to give a frequency dependent seismic moment estimate in the 1-5 Hz frequency band analyzed here. If this is true, then the source spectrum shape would provide a discriminant between extended and point sources in addition to the currently known ripple firing scalloping effect on body wave arrivals. Note that the surface wave technique focuses on the spectral shape within a narrow frequency band and does not have the band width necessary to identify spectral minima.

Table 3
Source Parameters of Nuclear (N) and Chemical (C) explosions

Type	ID	Y (ton)	M_I $(dyne\text{-}cm)$	Ψ_∞ (m^3)	Ref
C	KQ01	0.5	2.37e+18	0.46	(Johnson, 1989)
C	KQ03	0.45	1.78e+18	0.53	(Johnson, 1989)
C	KQ05	0.45	1.99e+18	0.87	(Johnson, 1989)
C	KQ08	0.17	0.79e+18	0.42	(Johnson, 1989)
C	KQ09	0.15	0.75e+18	0.27	(Johnson, 1989)
C	ST87	0.125	2.87e+16	0.28	(Stump, 1987)
C	ST87	0.125	1.35e+16	0.11	(Stump, 1987)
C	ST87	0.125	0.94e+16	0.07	(Stump, 1987)
N	GASBUGGY	29000	2.57e+22	6371	(Perret, 1972)
N	HARZER	107000	7.40e+22	27000	(Johnson, 1988)
N	CHANCELLOR	78000	5.70e+22	21000	(Johnson, 1988)
C	NRDC3	10.0	4.00e+19	3.27	(Given *et al*, 1990)
C	SP1+	1.0	1.85e+18	0.29	(Ghassan, 1991)
C	SP4+	1.0	1.42e+18	0.20	(Ghassan, 1991)
C	SP6-	1.0	2.87e+18	0.47	(Ghassan, 1991)
C	SP6+	1.0	1.99e+18	0.36	(Ghassan, 1991)
C	SP13-	1.0	1.49e+18	0.28	(Ghassan, 1991)
C	SP20+	1.0	2.27e+18	0.30	(Ghassan, 1991)
C	SP19-	1.0	2.39e+18	0.46	(Ghassan, 1991)
C	SP19+	1.0	2.11e+18	0.35	(Ghassan, 1991)
N	NTSY-0.02	20	1.43e+19	11.0	(Bache, 1982)
N	NTSP-0.02	20	2.45e+19	9.6	(Bache, 1982)
N	NTSMM-60	60000	3.26e+22	25000	(Bache, 1982)

Data Source

KQ01, KQ03, KQ05, KQ08, KQ09. Inversion Kaiser quarry data with distance ranges of 70-600m by inversion of entire waveform for moment tensor elements. Low frequency level isotropic moment rates are used. Ψ_∞ taken from their Figure 40 moment tensor results.

SP1+, SP4+, SP6-, SP6+, SP13-, SP20+, SP19-, SP19+. Inversion of surface wave data from USGS refraction lines in Maine. The number indicates the shot point, and the plus (+) or minus (-) indicate whether the line went from the shot point to the next larger shot point (+), or to the next lower shot point number (-). A split recording spread was used. Q_β and shear-wave velocity profiles are determined. M_I is estimated by a regression of filtered synthetic and observed seismic traces over the entire data range. Filter bands of 0.5-1.5 Hz, 1.5-2.5 Hz, 2.5-3.5 Hz, 3.4-4.5 Hz, and 0.5-4.5 Hz were used to test the correctness of the assumption of a step source time function for the isotropic source. Ψ_∞ derived using the earth model derived, using $M_I = 4\pi\rho\alpha^2\Psi_\infty$.

STUMP. Ψ_∞ and M_I from 50-150m varying half-space, 50-75 m layered and 50-100 m layered models in his Table 3.

GASBUGGY. Ψ_∞ estimated from four RDP's in his Figure 7. M_I derived from each Ψ_∞ using $M_I = 4\pi\rho\alpha^2\Psi_\infty$ with ρ and α given in his Table 1. The yield is given at 29 kT in the paper.

HARZER and CHANCELLOR. Yield estimated from body wave, Ψ_∞ and M_I are an average of using four source models (Mueller-Murphy, von Seggern-Blandford, Helmberger-Hadley, and Haskell) (Johnson, 1988). Johnson (1988) notes the presence of spall.

NRDC3. M_0 estimated from vertical component Lg spectra published in Given *et al* (1990). Ψ_∞ derived using the earth model provided. Sereno (1990) estimated an explosion moment of 5.0E+20 dyne-cm for the calibration shot, no correction is made for free surface effects. This observation is not plotted, but would be a major outlier!

NTSY-0.02, NTSP-0.02, NTSMM-60. From Bache (1982) Ψ_∞ values for scaled 0.02 kT nuclear shots at Yucca (NTSY-0.02) and Pahute (NTSP-0.02) and for Mueller/Murphy wet tuff/rhyolite 60 kT (NTSMM-60). To obtain isotropic moment, ρ = 1.8 and 2.0 gm/cc and α = 2.4 and 3.5 km/sec for Yucca and Pahute, respectively (Bache *et al.*, 1978).

REFERENCES

Bache, T. C. (1982). Estimating the yield of underground nuclear explosions, *Bull. Seism. Soc. Am.* 72 S131-S168.

Bache, T. C., W. L. Rodi, and D. G. Harkrider (1978). Crustal structures

inferred from Rayleigh wave signatures of NTS explosions, *Bull. Seism. Soc. Am.* **68** 1399-1413.

Given, H. K., N. T. Tarasov, V. Zhuravlev, F. L. Vernon, J. Berger and I. L. Nersesov (1990). High-frequency seismic observations in Eastern Kazakhstan, USSR, with emphasis on chemical explosion experiments, *J. Geophys. Res.* **95**, 295-307.

Johnson, L. R. and M. A. Leonard (1989). Near-source observations of quarry explosions, in McEvilly, T. V., and L. R. Johnson (1989), *Regional studies with broadband data*, Geophysics Laboratory GL-TR-89-0224, pp 1-57.

Johnson, L. R. (1988). Source characteristics of two underground nuclear explosions, *Geophys J.* **95**, 15-30.

Keilis-Borok, V. I., A. L. Levshin, T. B. Yanovskaya, A. V. Lander, B. G. Bukchin, M. P. Barmin, L. I. Ratnikova, and E. N. Its (1989). *Seismic surface waves in a laterally inhomogeneous earth*, Kluwer Academic Publishers, Dordrecht.

Murphy, J. M. and J. H. Luetgert (1986). Data report for the Maine-Quebec cross-strike seismic-refraction profile, *U. S. Geological Survey Open-File Report 86-47*, Menlo Park, CA.

Murphy, J. M. and J. H. Luetgert (1987). Data report for the Maine along-strike seismic-refraction profiles, *U. S. Geological Survey Open-File Report 87-133*, Menlo Park, CA.

Nolet, G. (1990). Partitioned waveform inversion and two-dimensional structure under the network of autonomously recording seismographs, *J. Geophys. Res.* **95**, 8499-8512.

Perret, W. R. (1972). Gasbuggy seismic source experiments, *Geophysics* **37**, 301-312.

Soreno, T. J. (1990). Frequency-dependent attenuation in Eastern Kazakhstan and implications for seismic detection thresholds in the Soviet Union, *Bull. Seism. Soc. Am.* **80**, 2089-2105.

Stump, B. W. (1987). Mathematical representation and physical interpretation of a contained chemical explosion in alluvium, *Bull. Seism. Soc. Am.* **77**, 1312-1325.

DISTRIBUTION LIST

Prof. Thomas Ahrens
Seismological Lab, 252-21
Division of Geological & Planetary Sciences
California Institute of Technology
Pasadena, CA 91125

Prof. Keiiti Aki
Center for Earth Sciences
University of Southern California
University Park
Los Angeles, CA 90089-0741

Prof. Shelton Alexander
Geosciences Department
403 Deike Building
The Pennsylvania State University
University Park, PA 16802

Dr. Ralph Alewine, III
DARPA/NMRO
3701 North Fairfax Drive
Arlington, VA 22203-1714

Prof. Charles B. Archambeau
CIRES
University of Colorado
Boulder, CO 80309

Dr. Thomas C. Bache, Jr.
Science Applications Int'l Corp.
10260 Campus Point Drive
San Diego, CA 92121 (2 copies)

Prof. Muawia Barazangi
Institute for the Study of the Continent
Cornell University
Ithaca, NY 14853

Dr. Jeff Barker
Department of Geological Sciences
State University of New York
at Binghamton
Vestal, NY 13901

Dr. Douglas R. Baumgardt
ENSCO, Inc
5400 Port Royal Road
Springfield, VA 22151-2388

Dr. Susan Beck
Department of Geosciences
Building #77
University of Arizona
Tucson, AZ 85721

Dr. T.J. Bennett
S-CUBED
A Division of Maxwell Laboratories
11800 Sunrise Valley Drive, Suite 1212
Reston, VA 22091

Dr. Robert Blandford
AFTAC/TT, Center for Seismic Studies
1300 North 17th Street
Suite 1450
Arlington, VA 22209-2308

Dr. G.A. Bollinger
Department of Geological Sciences
Virginia Polytechnical Institute
21044 Derring Hall
Blacksburg, VA 24061

Dr. Stephen Bratt
Center for Seismic Studies
1300 North 17th Street
Suite 1450
Arlington, VA 22209-2308

Dr. Lawrence Burdick
Woodward-Clyde Consultants
566 El Dorado Street
Pasadena, CA 91109-3245

Dr. Robert Burridge
Schlumberger-Doll Research Center
Old Quarry Road
Ridgefield, CT 06877

Dr. Jerry Carter
Center for Seismic Studies
1300 North 17th Street
Suite 1450
Arlington, VA 22209-2308

Dr. Eric Chael
Division 9241
Sandia Laboratory
Albuquerque, NM 87185

Prof. Vernon F. Cormier
Department of Geology & Geophysics
U-45, Room 207
University of Connecticut
Storrs, CT 06268

Prof. Steven Day
Department of Geological Sciences
San Diego State University
San Diego, CA 92182

ırvin Denny
S. Department of Energy
fice of Arms Control
ıshington, DC 20585

. Zoltan Der
ISCO, Inc.
)0 Port Royal Road
ringfield, VA 22151-2388

)f. Adam Dziewonski
ıffman Laboratory, Harvard University
pt. of Earth Atmos. & Planetary Sciences
Oxford Street
mbridge, MA 02138

)f. John Ebel
partment of Geology & Geophysics
ston College
estnut Hill, MA 02167

c Fielding
EE Hall
STOC
rnell University
aca, NY 14853

. Mark D. Fisk
ssion Research Corporation
5 State Street
). Drawer 719
ıta Barbara, CA 93102

f Stanley Flatte
plied Sciences Building
iversity of California, Santa Cruz
ıta Cruz, CA 95064

John Foley
R-Geo Sciences
)0 Crown Colony Drive
incy, MA 02169

)f. Donald Forsyth
partment of Geological Sciences
)wn University
ovidence, RI 02912

Art Frankel
). Geological Survey
National Center
ston, VA 22092

Dr. Cliff Frolich
Institute of Geophysics
8701 North Mopac
Austin, TX 78759

Dr. Holly Given
IGPP, A-025
Scripps Institute of Oceanography
University of California, San Diego
La Jolla, CA 92093

Dr. Jeffrey W. Given
SAIC
10260 Campus Point Drive
San Diego, CA 92121

Dr. Dale Glover
Defense Intelligence Agency
ATTN: ODT-1B
Washington, DC 20301

Dr. Indra Gupta
Teledyne Geotech
314 Montgomery Street
Alexanderia, VA 22314

Dan N. Hagedon
Pacific Northwest Laboratories
Battelle Boulevard
Richland, WA 99352

Dr. James Hannon
Lawrence Livermore National Laboratory
P.O. Box 808
L-205
Livermore, CA 94550

Dr. Roger Hansen
HQ AFTAC/TTR
Patrick AFB, FL 32925-6001

Prof. David G. Harkrider
Seismological Laboratory
Division of Geological & Planetary Sciences
California Institute of Technology
Pasadena, CA 91125

Prof. Danny Harvey
CIRES
University of Colorado
Boulder, CO 80309

Prof. Donald V. Helmberger
Seismological Laboratory
Division of Geological & Planetary Sciences
California Institute of Technology
Pasadena, CA 91125

Prof. Eugene Herrin
Institute for the Study of Earth and Man
Geophysical Laboratory
Southern Methodist University
Dallas, TX 75275

Prof. Robert B. Herrmann
Department of Earth & Atmospheric Sciences
St. Louis University
St. Louis, MO 63156

Prof. Lane R. Johnson
Seismographic Station
University of California
Berkeley, CA 94720

Prof. Thomas H. Jordan
Department of Earth, Atmospheric &
Planetary Sciences
Massachusetts Institute of Technology
Cambridge, MA 02139

Prof. Alan Kafka
Department of Geology & Geophysics
Boston College
Chestnut Hill, MA 02167

Robert C. Kemerait
ENSCO, Inc.
445 Pineda Court
Melbourne, FL 32940

Dr. Max Koontz
U.S. Dept. of Energy/DP 5
Forrestal Building
1000 Independence Avenue
Washington, DC 20585

Dr. Richard LaCoss
MIT Lincoln Laboratory, M-200B
P.O. Box 73
Lexington, MA 02173-0073

Dr. Fred K. Lamb
University of Illinois at Urbana-Champaign
Department of Physics
1110 West Green Street
Urbana, IL 61801

Prof. Charles A. Langston
Geosciences Department
403 Deike Building
The Pennsylvania State University
University Park, PA 16802

Jim Lawson, Chief Geophysicist
Oklahoma Geological Survey
Oklahoma Geophysical Observatory
P.O. Box 8
Leonard, OK 74043-0008

Prof. Thorne Lay
Institute of Tectonics
Earth Science Board
University of California, Santa Cruz
Santa Cruz, CA 95064

Dr. William Leith
U.S. Geological Survey
Mail Stop 928
Reston, VA 22092

Mr. James F. Lewkowicz
Phillips Laboratory/GPEH
Hanscom AFB, MA 01731-5000(2 copies)

Mr. Alfred Lieberman
ACDA/VI-OA State Department Building
Room 5726
320-21st Street, NW
Washington, DC 20451

Prof. L. Timothy Long
School of Geophysical Sciences
Georgia Institute of Technology
Atlanta, GA 30332

Dr. Randolph Martin, III
New England Research, Inc.
76 Olcott Drive
White River Junction, VT 05001

Dr. Robert Masse
Denver Federal Building
Box 25046, Mail Stop 967
Denver, CO 80225

Dr. Gary McCartor
Department of Physics
Southern Methodist University
Dallas, TX 75275

Prof. Thomas V. McEvilly
Seismographic Station
University of California
Berkeley, CA 94720

Dr. Art McGarr
U.S. Geological Survey
Mail Stop 977
U.S. Geological Survey
Menlo Park, CA 94025

Dr. Keith L. McLaughlin
S-CUBED
A Division of Maxwell Laboratory
P.O. Box 1620
La Jolla, CA 92038-1620

Stephen Miller & Dr. Alexander Florence
SRI International
333 Ravenswood Avenue
Box AF 116
Menlo Park, CA 94025-3493

Prof. Bernard Minster
IGPP, A-025
Scripps Institute of Oceanography
University of California, San Diego
La Jolla, CA 92093

Prof. Brian J. Mitchell
Department of Earth & Atmospheric Sciences
St. Louis University
St. Louis, MO 63156

Mr. Jack Murphy
S-CUBED
A Division of Maxwell Laboratory
11800 Sunrise Valley Drive, Suite 1212
Reston, VA 22091 (2 Copies)

Dr. Keith K. Nakanishi
Lawrence Livermore National Laboratory
L-025
P.O. Box 808
Livermore, CA 94550

Dr. Carl Newton
Los Alamos National Laboratory
P.O. Box 1663
Mail Stop C335, Group ESS-3
Los Alamos, NM 87545

Dr. Bao Nguyen
HQ AFTAC/TTR
Patrick AFB, FL 32925-6001

Prof. John A. Orcutt
IGPP, A-025
Scripps Institute of Oceanography
University of California, San Diego
La Jolla, CA 92093

Prof. Jeffrey Park
Kline Geology Laboratory
P.O. Box 6666
New Haven, CT 06511-8130

Dr. Howard Patton
Lawrence Livermore National Laboratory
L-025
P.O. Box 808
Livermore, CA 94550

Dr. Frank Pilotte
HQ AFTAC/TT
Patrick AFB, FL 32925-6001

Dr. Jay J. Pulli
Radix Systems, Inc.
2 Taft Court, Suite 203
Rockville, MD 20850

Dr. Robert Reinke
ATTN: FCTVTD
Field Command
Defense Nuclear Agency
Kirtland AFB, NM 87115

Prof. Paul G. Richards
Lamont-Doherty Geological Observatory
of Columbia University
Palisades, NY 10964

Mr. Wilmer Rivers
Teledyne Geotech
314 Montgomery Street
Alexandria, VA 22314

Dr. George Rothe
HQ AFTAC/TTR
Patrick AFB, FL 32925-6001

Dr. Alan S. Ryall, Jr.
DARPA/NMRO
3701 North Fairfax Drive
Arlington, VA 22209-1714

Dr. Richard Sailor
TASC, Inc.
55 Walkers Brook Drive
Reading, MA 01867

Prof. Charles G. Sammis
Center for Earth Sciences
University of Southern California
University Park
Los Angeles, CA 90089-0741

Prof. Christopher H. Scholz
Lamont-Doherty Geological Observatory
of Columbia University
Palisades, CA 10964

Dr. Susan Schwartz
Institute of Tectonics
1156 High Street
Santa Cruz, CA 95064

Secretary of the Air Force
(SAFRD)
Washington, DC 20330

Office of the Secretary of Defense
DDR&E
Washington, DC 20330

Thomas J. Sereno, Jr.
Science Application Int'l Corp.
10260 Campus Point Drive
San Diego, CA 92121

Dr. Michael Shore
Defense Nuclear Agency/SPSS
6801 Telegraph Road
Alexandria, VA 22310

Dr. Matthew Sibol
Virginia Tech
Seismological Observatory
4044 Derring Hall
Blacksburg, VA 24061-0420

Prof. David G. Simpson
IRIS, Inc.
1616 North Fort Myer Drive
Suite 1440
Arlington, VA 22209

Donald L. Springer
Lawrence Livermore National Laboratory
L-025
P.O. Box 808
Livermore, CA 94550

Dr. Jeffrey Stevens
S-CUBED
A Division of Maxwell Laboratory
P.O. Box 1620
La Jolla, CA 92038-1620

Lt. Col. Jim Stobie
ATTN: AFOSR/NL
Bolling AFB
Washington, DC 20332-6448

Prof. Brian Stump
Institute for the Study of Earth & Man
Geophysical Laboratory
Southern Methodist University
Dallas, TX 75275

Prof. Jeremiah Sullivan
University of Illinois at Urbana-Champaign
Department of Physics
1110 West Green Street
Urbana, IL 61801

Prof. L. Sykes
Lamont-Doherty Geological Observatory
of Columbia University
Palisades, NY 10964

Dr. David Taylor
ENSCO, Inc.
445 Pineda Court
Melbourne, FL 32940

Dr. Steven R. Taylor
Los Alamos National Laboratory
P.O. Box 1663
Mail Stop C335
Los Alamos, NM 87545

Prof. Clifford Thurber
University of Wisconsin-Madison
Department of Geology & Geophysics
1215 West Dayton Street
Madison, WS 53706

Prof. M. Nafi Toksoz
Earth Resources Lab
Massachusetts Institute of Technology
42 Carleton Street
Cambridge, MA 02142

Dr. Larry Turnbull
CIA-OSWR/NED
Washington, DC 20505

Dr. Gregory van der Vink
IRIS, Inc.
1616 North Fort Myer Drive
Suite 1440
Arlington, VA 22209

Dr. Karl Veith
EG&G
5211 Auth Road
Suite 240
Suitland, MD 20746

Prof. Terry C. Wallace
Department of Geosciences
Building #77
University of Arizona
Tuscon, AZ 85721

Dr. Thomas Weaver
Los Alamos National Laboratory
P.O. Box 1663
Mail Stop C335
Los Alamos, NM 87545

Dr. William Wortman
Mission Research Corporation
8560 Cinderbed Road
Suite 700
Newington, VA 22122

Prof. Francis T. Wu
Department of Geological Sciences
State University of New York
at Binghamton
Vestal, NY 13901

AFTAC/CA
(STINFO)
Patrick AFB, FL 32925-6001

DARPA/PM
3701 North Fairfax Drive
Arlington, VA 22203-1714

DARPA/RMO/RETRIEVAL
3701 North Fairfax Drive
Arlington, VA 22203-1714

DARPA/RMO/SECURITY OFFICE
3701 North Fairfax Drive
Arlington, VA 22203-1714

HQ DNA
ATTN: Technical Library
Washington, DC 20305

Defense Intelligence Agency
Directorate for Scientific & Technical Intelligence
ATTN: DTIB
Washington, DC 20340-6158

Defense Technical Information Center
Cameron Station
Alexandria, VA 22314 (2 Copies)

TACTEC
Battelle Memorial Institute
505 King Avenue
Columbus, OH 43201 (Final Report)

Phillips Laboratory
ATTN: XPG
Hanscom AFB, MA 01731-5000

Phillips Laboratory
ATTN: GPE
Hanscom AFB, MA 01731-5000

Phillips Laboratory
ATTN: TSML
Hanscom AFB, MA 01731-5000

Phillips Laboratory
ATTN: SUL
Kirtland, NM 87117 (2 copies)

Dr. Michel Bouchon
I.R.I.G.M.-B.P. 68
38402 St. Martin D'Heres
Cedex, FRANCE

Dr. Michel Campillo
Observatoire de Grenoble
I.R.I.G.M.-B.P. 53
38041 Grenoble, FRANCE

Dr. Kin Yip Chun
Geophysics Division
Physics Department
University of Toronto
Ontario, CANADA

Prof. Hans-Peter Harjes
Institute for Geophysic
Ruhr University/Bochum
P.O. Box 102148
4630 Bochum 1, GERMANY

Prof. Eystein Husebye
NTNF/NORSAR
P.O. Box 51
N-2007 Kjeller, NORWAY

David Jepsen
Acting Head, Nuclear Monitoring Section
Bureau of Mineral Resources
Geology and Geophysics
G.P.O. Box 378, Canberra, AUSTRALIA

Ms. Eva Johannisson
Senior Research Officer
National Defense Research Inst.
P.O. Box 27322
S-102 54 Stockholm, SWEDEN

Dr. Peter Marshall
Procurement Executive
Ministry of Defense
Blacknest, Brimpton
Reading PG7-FRS, UNITED KINGDOM

Dr. Bernard Massinon, Dr. Pierre Mechler
Societe Radiomana
27 rue Claude Bernard
75005 Paris, FRANCE (2 Copies)

Dr. Svein Mykkeltveit
NTNT/NORSAR
P.O. Box 51
N-2007 Kjeller, NORWAY (3 Copies)

Prof. Keith Priestley
University of Cambridge
Bullard Labs, Dept. of Earth Sciences
Madingley Rise, Madingley Road
Cambridge CB3 OEZ, ENGLAND

Dr. Jorg Schlittenhardt
Federal Institute for Geosciences & Nat'l Res.
Postfach 510153
D-3000 Hannover 51, GERMANY

Dr. Johannes Schweitzer
Institute of Geophysics
Ruhr University/Bochum
P.O. Box 1102148
4360 Bochum 1, GERMANY